We are IntechOpen, the world's leading publisher of Open Access books Built by scientists, for scientists

6,900
Open access books available

185,000
International authors and editors

200M
Downloads

Our authors are among the

154
Countries delivered to

TOP 1%
most cited scientists

12.2%
Contributors from top 500 universities



WEB OF SCIENCE™

Selection of our books indexed in the Book Citation Index in Web of Science™ Core Collection (BKCI)

Interested in publishing with us?
Contact book.department@intechopen.com

Numbers displayed above are based on latest data collected.
For more information visit www.intechopen.com



6

Numerical Methods for Near-Field Acoustic Holography over Arbitrarily Shaped Surfaces

Nicolas P. Valdivia
Naval Research Laboratory
Washington, DC
United States of America

1. Introduction

This chapter is devoted to the numerical methods of the technique near-field acoustic holography (NAH) introduced by Williams & Maynard (1980). As explained in the book of Williams (1999), NAH has had a tremendous success analyzing source regions with geometries which conform closely to one of the separable geometries of the acoustic wave equation; for example, planar, cylindrical, and spherical geometries. In these analyses the pressure field radiated from an object is measured on an imaginary surface outside (for exterior problems) or inside (for interior problems) the source region. This measured pressure is transformed into a hologram of different frequencies that are used to reconstruct the acoustic field on the body of the source. The solution of this inverse problem in these geometries relies on the expansion of the pressure field in terms of a complete set of eigenfunctions along with a knowledge of the analytical form of the Neumann or Dirichlet Green's function. The reconstructions are very efficient, requiring only fractions of a second of computation time per frequency.
Source regions with boundaries which vary appreciably in shape from one of these separable geometries require numerical methods that will be based on boundary integral representations of the solution as in Colton & Kress (1983; 1992). This chapter discusses the available results in the acoustic literature for the integral representations and the numerical discretization methods, and finally the regularization methods used for this inverse problem.

2. Integral representations

Let G be a domain in $\mathbb{R}^3$, interior to the boundary surface Γ (as shown in Fig. 1) where we assume that Γ is allowed to have edges and corners. Similarly we will denote as G^+ the region outside of G that shares the same boundary Γ. For a time-harmonic ($e^{-i\omega t}$) disturbance of radial frequency ω the sound pressure p satisfies the homogeneous Helmholtz equation in G (or G^+)

$$\Delta p + k^2 p = 0, \tag{1}$$

where p is given in N/m^2 units, $k = \omega/c$ is the wave number and c the constant for the speed of sound given in m/s units. Here $\omega = 2\pi f$, f is the frequency given in Hz. A solution p that

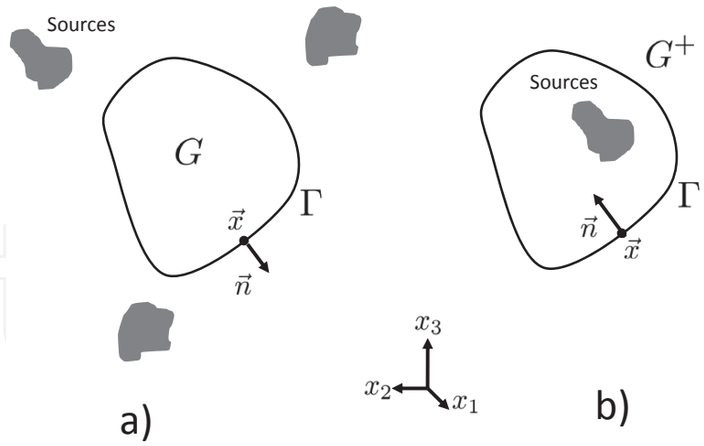


Fig. 1. Setup for the acoustic problem, a)interior problem and b)exterior problem.

satisfies Equation 1 in G^+ satisfies the Sommerfeld radiation condition

$$\lim_{r\to\infty} r\left\{\frac{\partial p}{\partial r} - ikp\right\} = 0, \quad r = |\vec{x}|, \tag{2}$$

where $\vec{x} = (x_1, x_2, x_3)$ and $|\vec{x}| = \sqrt{x_1^2 + x_2^2 + x_3^2}$.
At the boundary Γ the normal vibration v is related to the acoustic pressure p by Euler's equation

$$i\rho\omega v = \frac{\partial p}{\partial \vec{n}}, \tag{3}$$

where ρ is the mean fluid density given in kg/m^3 units and $\vec{n}$ is the vector unit normal with direction shown in Fig. 1.

2.1 Integral operators

We define the integral operators as in Colton & Kress (1983; 1992)

$$\left(S_\Gamma \varphi\right)(\vec{x}) := \int_\Gamma \Phi(\vec{x},\vec{y})\varphi(\vec{y})dS(\vec{y}), \quad \vec{x} \in \mathbb{R}^3, \tag{4}$$

$$\left(D_\Gamma \varphi\right)(\vec{x}) := \int_\Gamma \frac{\partial \Phi(\vec{x},\vec{y})}{\partial \vec{n}(\vec{y})}\varphi(\vec{y})dS(\vec{y}), \quad \vec{x} \in \mathbb{R}^3\backslash\Gamma, \tag{5}$$

$$\left(K_\Gamma \varphi\right)(\vec{x}) := \left(\frac{\partial S_\Gamma}{\partial \vec{n}}\varphi\right)(\vec{x}) := \int_\Gamma \frac{\partial \Phi(\vec{x},\vec{y})}{\partial \vec{n}(\vec{x})}\varphi(\vec{y})dS(\vec{y}), \quad \vec{x} \in \mathbb{R}^3\backslash\Gamma, \tag{6}$$

$$\left(H_\Gamma \varphi\right)(\vec{x}) := \left(\frac{\partial D_\Gamma}{\partial \vec{n}}\varphi\right)(\vec{x}) := \int_\Gamma \frac{\partial^2 \Phi(\vec{x},\vec{y})}{\partial \vec{n}(\vec{x})\partial \vec{n}(\vec{y})}\varphi(\vec{y})dS(\vec{y}), \quad \vec{x} \in \mathbb{R}^3\backslash\Gamma, \tag{7}$$

where Φ is the *free space Green's function* to the Helmholtz equation

$$\Phi(\vec{x},\vec{y}) = \frac{\exp\left(ik\left|\vec{x}-\vec{y}\right|\right)}{4\pi\left|\vec{x}-\vec{y}\right|}. \tag{8}$$

In this work we will not discuss the smoothness properties of the operators. A detailed description of these properties is given in Colton & Kress (1983) and McLean (2000). The most

important property for the purpose of NAH will be the evaluation of an operator S_Γ at $\vec{x} \in \Gamma$. We describe this as

$$(S_\Gamma \varphi)^{\pm}(\vec{x}) := \lim_{h \to 0} (S_\Gamma \varphi)(\vec{x} - h\vec{n}(\vec{x})),$$

where we will understand as the uppercase "$+$" the exterior problem with the direction of $\vec{n}$ as in Fig. 1b, while uppercase "$-$" the interior problem with the direction of $\vec{n}$ as in Fig. 1a. We keep this notation for all operators in Equations 4-7. Having explained the notation we have the *continuity relations*

$$(S_\Gamma \varphi)^{+}(\vec{x}) := (S_\Gamma \varphi)^{-}(\vec{x}), \tag{9}$$

$$(H_\Gamma \varphi)^{+}(\vec{x}) := (H_\Gamma \varphi)^{-}(\vec{x}), \tag{10}$$

and the *jump relations*

$$(D_\Gamma \varphi)^{\pm}(\vec{x}) := \int_\Gamma \frac{\partial \Phi(\vec{x}, \vec{y})}{\partial \vec{n}(\vec{y})} \varphi(\vec{y})\, dS(\vec{y}) \pm \Omega(\vec{x})\varphi(\vec{x}), \tag{11}$$

$$(K_\Gamma \varphi)^{\pm}(\vec{x}) := \int_\Gamma \frac{\partial \Phi(\vec{x}, \vec{y})}{\partial \vec{n}(\vec{x})} \varphi(\vec{y})\, dS(\vec{y}) \mp \Omega(\vec{x})\varphi(\vec{x}), \tag{12}$$

where $\Omega(\vec{x})$ is the solid angle coefficient given by the integral formula

$$\Omega(\vec{x}) = -\int_\Gamma \frac{\partial}{\partial \vec{n}(\vec{y})} \left(\frac{1}{4\pi |\vec{x} - \vec{y}|} \right) dS(\vec{y}), \quad \vec{x} \in \Gamma. \tag{13}$$

2.2 Integral formulations

The classical Helmholtz-Kirchhoff integral equation described in Colton & Kress (1983) is known as the integral representation of the pressure by the *direct formulation*. This classical representation has been used for purposes of solving NAH by several authors like Kim & Ih (1996; 2000); Kim & Lee (1990); Maynard (1988); Nelson & Yoon (2000); Sureshkumar & Raveendra (2001); Veronesi & Maynard (1989); Williams (2001); Yoon & Nelson (2000). The sound pressure in G^+ by the direct formulation has the integral representation

$$p(\vec{x}) = \begin{cases} i\rho\omega (S_\Gamma v)(\vec{x}) - (D_\Gamma p)(\vec{x}), & \vec{x} \in G^+, \\ 0, & \vec{x} \in G, \end{cases} \tag{14}$$

and in G

$$p(\vec{x}) = \begin{cases} 0, & \vec{x} \in G^+, \\ (D_\Gamma p)(\vec{x}) - i\rho\omega (S_\Gamma v)(\vec{x}), & \vec{x} \in G. \end{cases} \tag{15}$$

The *indirect formulations* are based on representations to the solution of Equation 1 like the single source or double source representation found in Augusztinovicz (1999); Delillo et al. (2000); DeLillo et al. (2001; 2003); Raveendra et al. (1998); Schuhmacher et al. (2003); Tekatlian et al. (1996); Vlahopoulos & Raveerdra (1998); Williams et al. (2000); Zhang et al. (2001; 2000). Using the notation of the previous subsection the single source representation is defined as

$$p(\vec{x}) = (S_\Gamma \varphi)(\vec{x}), \quad \vec{x} \in \mathbb{R}^3, \tag{16}$$

where φ is the density function, the double source representation

$$p(\vec{x}) = (D_\Gamma \varphi)(\vec{x}), \quad \vec{x} \in \mathbb{R}^3 \backslash \Gamma. \tag{17}$$

and the combination of sources

$$p(\vec{x}) = \left([S_\Gamma + i\eta D_\Gamma]\varphi\right)(\vec{x}), \quad \vec{x} \in \mathbb{R}^3 \backslash \Gamma, \tag{18}$$

where η is a constant.

2.3 Boundary maps

We define the well-known Dirichlet-to-Neumann γ_{dn} and Neumann-to-Dirichlet γ_{nd} boundary operators for $\vec{x} \in \Gamma$

$$p(\vec{x}) = \left(\gamma_{nd} v\right)^{\pm}(\vec{x}), \quad v(\vec{x}) = \left(\gamma_{dn} p\right)^{\pm}(\vec{x}). \tag{19}$$

For the direct formulation we found that

$$\begin{aligned} \left(\gamma_{nd}\phi\right)^{\pm}(\vec{x}) &:= i\rho\omega \left(\left[D_\Gamma^{\pm} \pm I\right]^{-1} S_\Gamma^{\pm} \phi \right)(\vec{x}), \\ \left(\gamma_{dn}\phi\right)^{\pm}(\vec{x}) &:= \frac{1}{i\rho\omega} \left(\left(S_\Gamma^{\pm}\right)^{-1} \left[D_\Gamma^{\pm} \pm I\right] \phi \right)(\vec{x}), \end{aligned} \tag{20}$$

where I is the identity operator. For the indirect formulation with single source formulation we have the relations

$$\begin{aligned} \left(\gamma_{nd}\phi\right)^{\pm}(\vec{x}) &:= i\rho\omega \left(S_\Gamma^{\pm} \left(K_\Gamma^{\pm}\right)^{-1} \phi \right)(\vec{x}), \\ \left(\gamma_{dn}\phi\right)^{\pm}(\vec{x}) &:= \frac{1}{i\rho\omega} \left(K_\Gamma^{\pm} \left(S_\Gamma^{\pm}\right)^{-1} \phi \right)(\vec{x}), \end{aligned} \tag{21}$$

for the indirect formulation with double source formulation

$$\begin{aligned} \left(\gamma_{nd}\phi\right)^{\pm}(\vec{x}) &:= i\rho\omega \left(D_\Gamma^{\pm} \left(H_\Gamma^{\pm}\right)^{-1} \phi \right)(\vec{x}), \\ \left(\gamma_{dn}\phi\right)^{\pm}(\vec{x}) &:= \frac{1}{i\rho\omega} \left(H_\Gamma^{\pm} \left(D_\Gamma^{\pm}\right)^{-1} \phi \right)(\vec{x}), \end{aligned} \tag{22}$$

and for the indirect formulation with a combination of sources

$$\begin{aligned} \left(\gamma_{nd}\phi\right)^{\pm}(\vec{x}) &:= i\rho\omega \left(\left(S_\Gamma^{\pm} + i\eta D_\Gamma^{\pm}\right) \left(K_\Gamma^{\pm} + i\eta H_\Gamma^{\pm}\right)^{-1} \phi \right)(\vec{x}), \\ \left(\gamma_{dn}\phi\right)^{\pm}(\vec{x}) &:= \frac{1}{i\rho\omega} \left(\left(K_\Gamma^{\pm} + i\eta H_\Gamma^{\pm}\right) \left(S_\Gamma^{\pm} + i\eta D_\Gamma^{\pm}\right)^{-1} \phi \right)(\vec{x}). \end{aligned} \tag{23}$$

2.4 Transfer functions

The traditional approach for solving NAH (both for direct and indirect formulations) is based on the operators

$$p(\vec{x}) = \left(\mathcal{G}_\Gamma^d p\right)(\vec{x}) := \int_\Gamma \Phi_d(\vec{x}, \vec{y}) p(\vec{y}) dS(\vec{y}), \quad \vec{x} \in \mathbb{R}^3 \backslash \Gamma, \tag{24}$$

$$p(\vec{x}) = \left(\mathcal{G}_\Gamma^n v\right)(\vec{x}) := \int_\Gamma \Phi_n(\vec{x}, \vec{y}) v(\vec{y}) dS(\vec{y}), \quad \vec{x} \in \mathbb{R}^3 \backslash \Gamma, \tag{25}$$

where the functions Φ_d and Φ_n are respectively the *Dirichlet Green's function* and *Neumann Green's function* for Equation 1. These integral equations are similar to the Rayleigh's integral formulas for planar NAH (see Williams (1999)). In general, the knowledge of an explicit

formula for these Green's functions will be helpful, but can only be found for some restricted geometries (see Ouellet et al. (1991); Pan & Bies (1990); Williams (1997)).
With the help of the Dirichlet-to-Neumann γ_{dn} and Neumann-to-Dirichlet γ_{nd} boundary operators we can find an explicit representation of the operators $\mathcal{G}_\Gamma^d, \mathcal{G}_\Gamma^n$ for the direct formulations

$$\begin{aligned} \left(\mathcal{G}_\Gamma^d \varphi\right)^\pm (\vec{x}) &:= \left(\pm\left[i\rho\omega S_\Gamma\left(\gamma_{nd}^\pm\right) - D_\Gamma\right]\varphi\right)(\vec{x}), \\ \left(\mathcal{G}_\Gamma^n \varphi\right)^\pm (\vec{x}) &:= \left(\pm\left[i\rho\omega S_\Gamma - D_\Gamma\left(\gamma_{dn}^\pm\right)\right]\varphi\right)(\vec{x}). \end{aligned} \tag{26}$$

The indirect formulations with single source will have the expressions

$$\begin{aligned} \left(\mathcal{G}_\Gamma^d \varphi\right)^\pm (\vec{x}) &:= \left(S_\Gamma\left(S_\Gamma^\pm\right)^{-1}\varphi\right)(\vec{x}), \\ \left(\mathcal{G}_\Gamma^n \varphi\right)^\pm (\vec{x}) &:= i\rho\omega\left(S_\Gamma\left(K_\Gamma^\pm\right)^{-1}\varphi\right)(\vec{x}). \end{aligned} \tag{27}$$

for the double source

$$\begin{aligned} \left(\mathcal{G}_\Gamma^d \varphi\right)^\pm (\vec{x}) &:= \left(D_\Gamma\left(D_\Gamma^\pm\right)^{-1}\varphi\right)(\vec{x}), \\ \left(\mathcal{G}_\Gamma^n \varphi\right)^\pm (\vec{x}) &:= i\rho\omega\left(D_\Gamma\left(H_\Gamma^\pm\right)^{-1}\varphi\right)(\vec{x}). \end{aligned} \tag{28}$$

and for a combination of sources

$$\begin{aligned} \left(\mathcal{G}_\Gamma^d \varphi\right)^\pm (\vec{x}) &:= \left(\left(S_\Gamma + i\eta D_\Gamma\right)\left(S_\Gamma^\pm + i\eta D_\Gamma^\pm\right)^{-1}\varphi\right)(\vec{x}), \\ \left(\mathcal{G}_\Gamma^n \varphi\right)^\pm (\vec{x}) &:= i\rho\omega\left(\left(S_\Gamma + i\eta D_\Gamma\right)\left(K_\Gamma^\pm + i\eta H_\Gamma^\pm\right)^{-1}\varphi\right)(\vec{x}). \end{aligned} \tag{29}$$

3. Numerical methods for integral equations

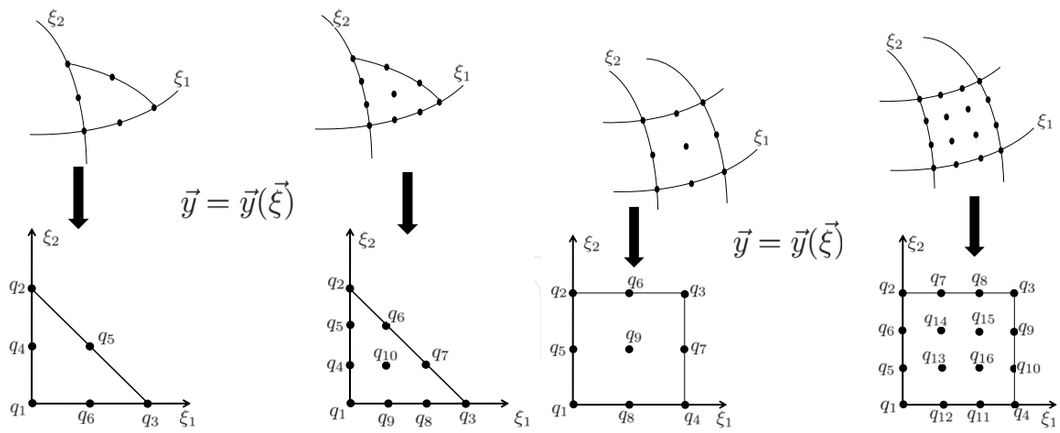
The numerical solution of an integral equation is based on its discretization, which is a reduction into a linear matrix system where numerical methods can be applied. Boundary Element Methods (BEM) have been successfully used in the area of acoustic radiation and scattering (see Bai (1992); Kang & Ih (2000a); Kim & Ih (1996); Langrenne & Garcia (1999); Seybert et al. (1985); Williams et al. (2000)) for three dimensional surfaces.

3.1 Boundary integral methods

The boundary elements used for approximating the surface integral are schematically shown in Fig. 2. N_v triangular or quadrilateral elements are used in this study for the construction of meshes. The global cartesian coordinates $\vec{y}$ on any point of an element $\triangle_j, j = 1, ..., N_v$ are assumed to be related to the nodes $\vec{y}_{(m,j)}$, $m = 1, .., n_q$ by

$$\vec{y}(\vec{\xi}) = \sum_{m=1}^{n_q} N_m(\vec{\xi})\vec{y}_{(m,j)} \tag{30}$$

in which $\vec{\xi} = (\xi_1, \xi_2)$ and shape functions $N_m(\vec{\xi})$ for the triangular elements are given in Table 1 and for quadrilateral elements are given in Table 2.
Equation 30 is an isoparametric transformation in which a surface element is mapped into a plane equilateral unit triangle or quadrilateral (as in the lower part of figure 2). Next, the



(a) triangular elements (b) quadrilateral elements

Fig. 2. Boundary elements used for iso-parametric transformation: linear, quadratic and cubic elements.

	Linear	Quadratic	Cubic
$N_1(\vec{\xi})$	u	$u(2u-1)$	$\frac{1}{2}u(3u-1)(3u-2)$
$N_2(\vec{\xi})$	ξ_2	$\xi_2(2\xi_2-1)$	$\frac{1}{2}\xi_2(3\xi_2-1)(3\xi_2-2)$
$N_3(\vec{\xi})$	ξ_1	$\xi_1(2\xi_1-1)$	$\frac{1}{2}\xi_1(3\xi_1-1)(3\xi_1-2)$
$N_4(\vec{\xi})$		$4\xi_2 u$	$\frac{9}{2}\xi_2(3u-1)u$
$N_5(\vec{\xi})$		$4\xi_1\xi_2$	$\frac{9}{2}\xi_2(3\xi_2-1)u$
$N_6(\vec{\xi})$		$4\xi_1 u$	$\frac{9}{2}\xi_1\xi_2(3\xi_2-1)$
$N_7(\vec{\xi})$			$\frac{9}{2}\xi_1(3\xi_1-1)\xi_2$
$N_8(\vec{\xi})$			$\frac{9}{2}\xi_1(3\xi_1-1)u$
$N_9(\vec{\xi})$			$\frac{9}{2}\xi_1(3u-1)u$
$N_{10}(\vec{\xi})$			$27\xi_1\xi_2 u$
	$u = 1-\xi_1-\xi_2$		
	$q_1=(0,0)$, $q_2=(0,1)$, $q_3=(1,0)$,	$q_4=(0,\frac{1}{2})$, $q_5=(\frac{1}{2},\frac{1}{2})$, $q_6=(\frac{1}{2},0)$	$q_4=(0,\frac{1}{3})$, $q_5=(0,\frac{2}{3})$ $q_6=(\frac{1}{3},\frac{2}{3})$, $q_7=(\frac{2}{3},\frac{1}{3})$ $q_8=(\frac{2}{3},0)$, $q_9=(\frac{1}{3},0)$ $q_{10}=(\frac{1}{3},\frac{1}{3})$,

Table 1. Shape functions for triangular elements.

boundary variable φ given in Equations 4-7 and Equations 9-12 will be represented on each element j according to

$$\varphi(\vec{\xi}) = \sum_{m=1}^{n_q} N_m(\vec{\xi})\varphi_{(m,j)} \tag{31}$$

where $\varphi_{(m,j)}$ are the values of φ at node m of the element j.

	Linear	Quadratic	Cubic
$N_1(\vec{\xi})$	$\frac{1}{4}(1-\xi_1)(1-\xi_2)$	$\frac{1}{4}\xi_1(\xi_1-1)\xi_2(\xi_2-1)$	$\frac{81}{256}(\xi_1^2-\frac{1}{9})(\xi_2^2-\frac{1}{9})(\xi_1-1)(\xi_2-1)$
$N_2(\vec{\xi})$	$\frac{1}{4}(1-\xi_1)(1+\xi_2)$	$\frac{1}{4}\xi_1(\xi_1-1)\xi_2(1+\xi_2)$	$\frac{81}{256}(\xi_1^2-\frac{1}{9})(\xi_2^2-\frac{1}{9})(1-\xi_1)(\xi_2+1)$
$N_3(\vec{\xi})$	$\frac{1}{4}(1+\xi_1)(1+\xi_2)$	$\frac{1}{4}\xi_1(1+\xi_1)\xi_2(1+\xi_2)$	$\frac{81}{256}(\xi_1^2-\frac{1}{9})(\xi_2^2-\frac{1}{9})(\xi_1+1)(\xi_2+1)$
$N_4(\vec{\xi})$	$\frac{1}{4}(1+\xi_1)(1-\xi_2)$	$\frac{1}{4}\xi_1(1+\xi_1)\xi_2(\xi_2-1)$	$\frac{81}{256}(\xi_1^2-\frac{1}{9})(\xi_2^2-\frac{1}{9})(\xi_1+1)(1-\xi_2)$
$N_5(\vec{\xi})$		$\frac{1}{2}\xi_1(\xi_1-1)(1-\xi_2^2)$	$\frac{243}{256}(\xi_1^2-\frac{1}{9})(\xi_2^2-1)(1-\xi_1)(\xi_2-\frac{1}{3})$
$N_6(\vec{\xi})$		$\frac{1}{2}(1-\xi_1^2)\xi_2(1+\xi_2)$	$\frac{243}{256}(\xi_1^2-\frac{1}{9})(\xi_2^2-1)(\xi_1-1)(\xi_2+\frac{1}{3})$
$N_7(\vec{\xi})$		$\frac{1}{2}\xi_1(1+\xi_1)(1-\xi_2^2)$	$\frac{243}{256}(\xi_1^2-1)(\xi_2^2-\frac{1}{9})(\xi_1-\frac{1}{3})(\xi_2+1)$
$N_8(\vec{\xi})$		$\frac{1}{2}(1-\xi_1^2)\xi_2(\xi_2-1)$	$\frac{243}{256}(1-\xi_1^2)(\xi_2^2-\frac{1}{9})(\xi_1+\frac{1}{3})(\xi_2+1)$
$N_9(\vec{\xi})$		$(1-\xi_1^2)(1-\xi_2^2)$	$\frac{243}{256}(\xi_1^2-\frac{1}{9})(1-\xi_2^2)(\xi_1+1)(\xi_2+\frac{1}{3})$
$N_{10}(\vec{\xi})$			$\frac{243}{256}(\xi_1^2-\frac{1}{9})(\xi_2^2-1)(\xi_1+1)(\xi_2-\frac{1}{3})$
$N_{11}(\vec{\xi})$			$\frac{243}{256}(\xi_1^2-1)(\xi_2^2-\frac{1}{9})(\xi_1+\frac{1}{3})(\xi_2-1)$
$N_{12}(\vec{\xi})$			$\frac{243}{256}(\xi_1^2-1)(\xi_2^2-\frac{1}{9})(\xi_1-\frac{1}{3})(1-\xi_2)$
$N_{13}(\vec{\xi})$			$\frac{729}{256}(\xi_1^2-1)(\xi_2^2-1)(\xi_1-\frac{1}{3})(\xi_2-\frac{1}{3})$
$N_{14}(\vec{\xi})$			$\frac{729}{256}(\xi_1^2-1)(\xi_2^2-1)(\frac{1}{3}-\xi_1)(\xi_2+\frac{1}{3})$
$N_{15}(\vec{\xi})$			$\frac{729}{256}(\xi_1^2-1)(\xi_2^2-1)(\xi_1+\frac{1}{3})(\xi_2+\frac{1}{3})$
$N_{16}(\vec{\xi})$			$\frac{729}{256}(\xi_1^2-1)(\xi_2^2-1)(\xi_1+\frac{1}{3})(\frac{1}{3}-\xi_2)$
	$q_1=(-1,-1)$, $q_2=(-1,1)$, $q_3=(1,1)$, $q_4=(1,-1)$	$q_5=(-1,0)$, $q_6=(0,1)$, $q_7=(1,0)$, $q_8=(0,-1)$, $q_9=(0,0)$	$q_5=(-1,-\frac{1}{3}$, $q_6=(-1,\frac{1}{3})$, $q_7=(-\frac{1}{3},1)$, $q_8=(\frac{1}{3},1)$, $q_9=(1,\frac{1}{3})$, $q_{10}=(1,-\frac{1}{3})$, $q_{11}=(\frac{1}{3},-1)$, $q_{12}=(-\frac{1}{3},-1)$, $q_{13}=(-\frac{1}{3},-\frac{1}{3})$, $q_{14}=(-\frac{1}{3},\frac{1}{3})$, $q_{15}=(\frac{1}{3},\frac{1}{3})$, $q_{16}=(\frac{1}{3},-\frac{1}{3})$

Table 2. Shape functions for quadrilateral elements.

For $\vec{x}\in\mathbb{R}^3\backslash\Gamma$ the integrals in Equations 4-7 are approximated by

$$(S\varphi)(\vec{x})\approx\sum_{j=1}^{N_v}\sum_{m=1}^{n_q}S^i_{(m,j)}\varphi_{(m,j)},\quad (D\varphi)(\vec{x})\approx\sum_{j=1}^{N_v}\sum_{m=1}^{n_q}D^i_{(m,j)}\varphi_{(m,j)},\tag{32}$$

$$(K\varphi)(\vec{x})\approx\sum_{j=1}^{N_v}\sum_{m=1}^{n_q}K^i_{(m,j)}\varphi_{(m,j)},\quad (H\varphi)(\vec{x})\approx\sum_{j=1}^{N_v}\sum_{m=1}^{n_q}H^i_{(m,j)}\varphi_{(m,j)},$$

where

$$S^i_{(m,j)}=\int_{\triangle}\Phi(\vec{x}_i,\vec{y}(\xi_1,\xi_2))N_m(\xi_1,\xi_2)J(\xi_1,\xi_2)d\xi_1d\xi_2,\tag{33}$$

$$D^i_{(m,j)}=\int_{\triangle}\frac{\partial\Phi(\vec{x}_i,\vec{y}(\xi_1,\xi_2))}{\partial\vec{n}(\vec{y}(\xi_1,\xi_2))}N_m(\xi_1,\xi_2)J(\xi_1,\xi_2)d\xi_1d\xi_2,\tag{34}$$

$$K^i_{(m,j)}=\int_{\triangle}\frac{\partial\Phi(\vec{x}_i,\vec{y}(\xi_1,\xi_2))}{\partial\vec{n}(\vec{x}_i)}N_m(\xi_1,\xi_2)J(\xi_1,\xi_2)d\xi_1d\xi_2,\tag{35}$$

$$H^i_{(m,j)}=\int_{\triangle}\frac{\partial^2\Phi(\vec{x}_i,\vec{y}(\xi_1,\xi_2))}{\partial\vec{n}(\vec{y}(\xi_1,\xi_2))\partial\vec{n}(\vec{x}_i)}N_m(\xi_1,\xi_2)J(\xi_1,\xi_2)d\xi_1d\xi_2,\tag{36}$$

in which $\triangle$ is the unit surface element, $J(\xi_1,\xi_2)$ is the Jacobian of the coordinate transformation. This Jacobian is known exactly for some surfaces, however for general

surfaces it is more convenient to approximate it numerically using Equation 30

$$J(\xi_1,\xi_2) \approx |\partial_{\xi_1} N_m(\xi_1,\xi_2) \times \partial_{\xi_2} N_m(\xi_1,\xi_2)|$$

as suggested in Chien (1995). Integrals $S^i_{(m,j)}$, $D^i_{(m,j)}$, $K^i_{(m,j)}$, $H^i_{(m,j)}$ are approximated numerically using the adaptive integration scheme given in (Atkinson, 1997, Chapter 9) with the formula $(T_2 : 5.1)$ from (Strout, 1971, Chapter 8) for triangles and gaussian quadrature for quadrilaterals.
For $\vec{x} \in \Gamma$ the integrals in Equations 9-12 will be approximated by

$$(D\varphi)^{\pm}(\vec{x}) \approx \sum_{j=1}^{N_v}\sum_{m=1}^{q} D^i_{(m,j)}\varphi_{(m,j)} \pm \Omega(\vec{x})\varphi(\vec{x}), \quad (S\varphi)(\vec{x})^{\pm} \approx \sum_{j=1}^{N_v}\sum_{m=1}^{n_q} S^i_{(m,j)}\varphi_{(m,j)}, \tag{37}$$

$$(K\varphi)^{\pm}(\vec{x}) \approx \sum_{j=1}^{N_v}\sum_{m=1}^{q} K^i_{(m,j)}\varphi_{(m,j)} \mp \Omega(\vec{x})\varphi(\vec{x}), \quad (H\varphi)(\vec{x})^{\pm} \approx \sum_{j=1}^{N_v}\sum_{m=1}^{n_q} H^i_{(m,j)}\varphi_{(m,j)},$$

Integrals $S^i_{(m,j)}$, $D^i_{(m,j)}$, $K^i_{(m,j)}$ and $H^i_{(m,j)}$ will be approximated using the adaptive integration scheme used for the previous case when $\vec{x} \notin \triangle_j$. When $\vec{x} \in \triangle_j$ then $S^i_{(m,j)}$, $D^i_{(m,j)}$, and $K^i_{(m,j)}$ are approximated numerically using a Duffy transformation and Gaussian quadrature as suggested in Schwab & Wendland (1992).

3.2 Equivalent sources methods

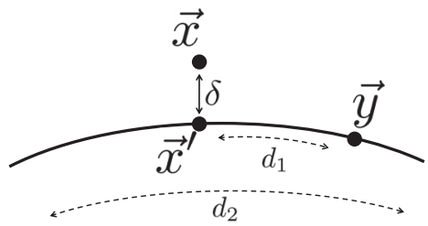


Fig. 3. Setup of integral approximation over element.

We utilize the notation of the previous subsection. The boundary variable φ given in Equations 4-7 will be represented on each element j as in Equation 31 using constant elements. The constant elements for triangular or quadrilateral shapes are

$$N_1(\vec{\xi}) = 1$$

and $q_1 = (1/3, 1/3)$ for triangular elements and $q_1 = (0,0)$ for quadrilateral elements.
For $\vec{x} \in \mathbb{R}^3 \backslash \Gamma$ the mean value theorem applied to Equation 32 gives

$$S^i_{(m,j)} = \Phi(\vec{x},\vec{\zeta})A_{\triangle}, \quad D^i_{(m,j)} = \frac{\partial\Phi(\vec{x},\vec{\zeta})}{\partial\vec{n}(\vec{\zeta})}A_{\triangle}, \tag{38}$$

$$K^i_{(m,j)} = \frac{\partial\Phi(\vec{x},\vec{\zeta})}{\partial\vec{n}(\vec{x})}A_{\triangle}, \quad D^i_{(m,j)} = \frac{\partial^2\Phi(\vec{x},\vec{\zeta})}{\partial\vec{n}(\vec{x})\partial\vec{n}(\vec{\zeta})}A_{\triangle},$$

for certain $\vec{\zeta} \in \triangle_j$ and

$$A_{\triangle_j} = \int_{\triangle} J(\xi_1,\xi_2)d\xi_1 d\xi_2,$$

The multi-dimensional Taylor series are used to expand around $\vec{y} \in \mathbb{R}^3$

$$\partial^{\alpha_1}_{\vec{n}(x)}\partial^{\alpha_2}_{\vec{n}(\vec{\zeta})}\Phi(\vec{x},\vec{\zeta}) = \partial^{\alpha_1}_{\vec{n}(\vec{x})}\partial^{\alpha_2}_{\vec{n}(\vec{y})}\Phi(\vec{x},\vec{y}) + D_1 + D_2 + ... \tag{39}$$

where $\alpha_1, \alpha_2 = 0, 1$ and

$$\begin{aligned} D_1 &= \sum_{m=1}^{3} \partial_{y_m}\left(\partial^{\alpha_1}_{\vec{n}(x)}\partial^{\alpha_2}_{\vec{n}(\vec{y})}\Phi(\vec{x},\vec{y})\right)(\zeta_m - y_m), \\ D_2 &= \sum_{m=1}^{3} \partial^2_{y_m}\left(\partial^{\alpha_1}_{\vec{n}(x)}\partial^{\alpha_2}_{\vec{n}(\vec{y})}\Phi(\vec{x},\vec{y})\right)\frac{(\zeta_m - y_m)^2}{2} \\ &\quad + \sum_{m,n=1,m\neq n}^{3} \partial_{y_m}\partial_{y_n}\left(\partial^{\alpha_1}_{x_i}\partial^{\alpha_2}_{\vec{n}(\vec{y})}\Phi(\vec{x},\vec{y})\right)(\zeta_m - y_m)(\zeta_n - y_n). \end{aligned}$$

From the derivatives of Φ we obtain the estimates

$$\left|\partial_{y_m}\partial^{\alpha_1}_{\vec{n}(\vec{x})}\partial^{\alpha_2}_{\vec{n}(\vec{y})}\Phi(\vec{x},\vec{y})\right| \leq \frac{A_{(1+\alpha_1+\alpha_2)}(k)}{4\pi|\vec{x}-\vec{y}|^{2+\alpha_1+\alpha_2}}, \quad \left|\partial_{y_m}\partial_{y_n}\partial^{\alpha_1}_{\vec{n}(\vec{x})}\partial^{\alpha_2}_{\vec{n}(\vec{y})}\Phi(\vec{x},\vec{y})\right| \leq \frac{A_{(2+\alpha_1+\alpha_2)}(k)}{4\pi|\vec{x}-\vec{y}|^{3+\alpha_1+\alpha_2}}$$

where

$$\begin{aligned} A_{(1)}(k) &= C_1(k), \quad A_{(2)}(k) = C_1(k) + C_2(k), \quad A_{(3)}(k) = 3C_2(k) + C_3(k), \\ A_{(4)}(k) &= 3C_2(k) + 4C_3(k) + C_4(k), \\ C_1(k) &= \left|ik|\vec{x}-\vec{y}| - 1\right|, \\ C_2(k) &= \left|k^2|\vec{x}-\vec{y}|^2 + 3ik|\vec{x}-\vec{y}| - 3\right|, \\ C_3(k) &= \left|ik^3|\vec{x}-\vec{y}|^3 - 6k^2|\vec{x}-\vec{y}|^2 - 15ik|\vec{x}-\vec{y}| + 15\right|, \\ C_4(k) &= \left|k^4|\vec{x}-\vec{y}|^4 + 10ik^3|\vec{x}-\vec{y}|^3 - 45k^2|\vec{x}-\vec{y}|^2 + 105ik|\vec{x}-\vec{y}| - 105\right|, \end{aligned}$$

We use the above estimates to obtain

$$\begin{aligned} |D_1| &\leq \frac{3A_{(1+\alpha_1+\alpha_2)}(k)}{4\pi}\frac{|\vec{y}-\vec{\zeta}|}{|\vec{x}-\vec{y}|^{2+\alpha_1+\alpha_2}} = \frac{3A_{(1+\alpha_1+\alpha_2)}(k)}{4\pi}\frac{|\vec{y}-\vec{\zeta}|}{|\vec{x}-\vec{y}|^{1+\alpha_1+\alpha_2}}\left(\frac{|\vec{y}-\vec{\zeta}|}{|\vec{x}-\vec{y}|}\right), \\ |D_2| &\leq \frac{9A_{(2+\alpha_1+\alpha_2)}(k)}{8\pi}\frac{|\vec{y}-\vec{\zeta}|^2}{|\vec{x}-\vec{y}|^{3+\alpha_1+\alpha_2}} = \frac{9A_{(2+\alpha_1+\alpha_2)}(k)}{8\pi}\frac{|\vec{y}-\vec{\zeta}|^2}{|\vec{x}-\vec{y}|^{1+\alpha_1+\alpha_2}}\left(\frac{|\vec{y}-\vec{\zeta}|}{|\vec{x}-\vec{y}|}\right)^2. \end{aligned}$$

It is not hard to observe from Fig. 3 that $\delta \leq |\vec{x}-\vec{y}| \leq \delta + d_1$ and $|\vec{y}-\vec{\zeta}| < \sqrt{2}d_2$ where d_2 is the arc-length distance of the element $\triangle_j$ and d_1 the distance between $\vec{x}$ and $\vec{x}'$ which is the projection of $\vec{x}$ into the element $\triangle_j$. Under the assumption that $\delta > \sqrt{2}d_2$ then we can utilize the approximation

$$\partial^{\alpha_1}_{\vec{n}(x)}\partial^{\alpha_2}_{\vec{n}(\vec{\zeta})}\Phi(\vec{x},\vec{\zeta}) = \partial^{\alpha_1}_{\vec{n}(\vec{x})}\partial^{\alpha_2}_{\vec{n}(\vec{y})}\Phi(\vec{x},\vec{y}) + \frac{3A_{(1+\alpha_1+\alpha_2)}(k)}{4\pi}\frac{|\vec{y}-\vec{\zeta}|}{|\vec{x}-\vec{y}|^{2+\alpha_1+\alpha_2}} + O\left(\frac{|\vec{y}-\vec{\zeta}|}{|\vec{x}-\vec{y}|}\right)^2. \tag{40}$$

The error estimate in Equation 40 has been studied in Valdivia & Williams (2006) for the case $\alpha_1 = \alpha_2 = 0$, $\delta < d_2 < 2\delta$. A similar behavior of the error should be expected for other cases

of α_1, α_2. Finally Equation 40 is used to justify the approximations of Equation 38 that results in the approximation

$$(S\varphi)(\vec{x}) \approx \sum_{j=1}^{N_v} \Phi(\vec{x}, \vec{y}_j) q_j, \tag{41}$$

$$(D\varphi)(\vec{x}) \approx \sum_{j=1}^{N_v} \frac{\partial \Phi(\vec{x}, \vec{y}_j)}{\partial \vec{n}(\vec{y}_j)} q_j, \tag{42}$$

$$(K\varphi)(\vec{x}) \approx \sum_{j=1}^{N_v} \frac{\partial \Phi(\vec{x}, \vec{y}_j)}{\partial \vec{n}(\vec{x})} q_j, \tag{43}$$

$$(H\varphi)(\vec{x}) \approx \sum_{j=1}^{N_v} \frac{\partial^2 \Phi(\vec{x}, \vec{y}_j)}{\partial \vec{n}(\vec{y}_j) \partial \vec{n}(\vec{x})} q_j, \tag{44}$$

where $q_j = \varphi_{(1,j)} S_{\triangle_j}$.

4. Near-field acoustic holography

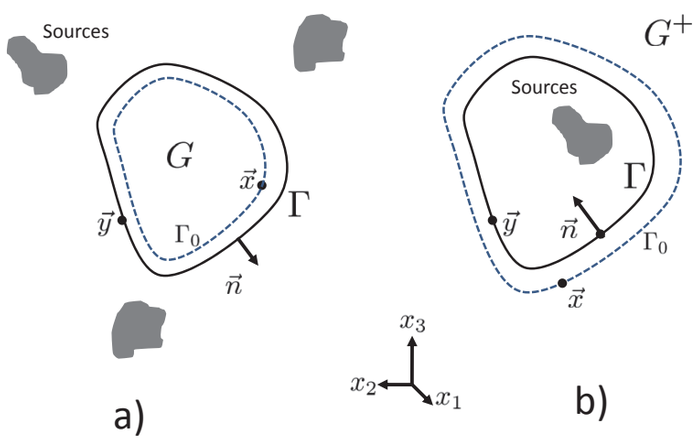


Fig. 4. Boundary setup for (a) interior NAH and (b) exterior NAH.

As shown in Fig. 4, for interior(exterior) NAH the acoustical sensors are placed on a surface Γ_0 inside (outside) the domain G. These are used to measure the pressure p and the fundamental problem is to recover the acoustic field (pressure, normal velocity and normal intensity) on Γ. The NAH problem for the *explicit approach* is reduced to the solution of the integral equations

$$\left(\mathcal{G}_\Gamma^d p\right)^{\pm}(\vec{x}) := p(\vec{x}), \quad \vec{x} \in \Gamma_0 \tag{45}$$

$$\left(\mathcal{G}_\Gamma^n v\right)^{\pm}(\vec{x}) := p(\vec{x}), \quad \vec{x} \in \Gamma_0. \tag{46}$$

The superscript sign "+" in Equations 45 and 46 is used for exterior NAH and "−" for interior NAH. This notation will be kept throughout the rest of this chapter.
In practice for the NAH technique we will take M pressure measurements on the surface Γ_0 and will want to recover N pressure or normal velocity points on the surface Γ. In general we will find that $M \geq N$, but there is no major theoretical contradiction if $M < N$. We will denote

as $\mathbf{p}$ the column vector with M pressure measurements on Γ_0. The N points of the recovered normal velocity and pressure on Γ will be given respectively by the column vectors $\mathbf{v}^s$, $\mathbf{p}^s$.

4.1 Boundary element methods

For each $\vec{x}_i \in \Gamma_0$ the sums in Equation 32 can be reduced for the N points on Γ to produce the $M \times M$ complex matrices $\left[\boldsymbol{\mathcal{S}}_{(\Gamma_0,\Gamma)}\right]$, $\left[\boldsymbol{\mathcal{D}}_{(\Gamma_0,\Gamma)}\right]$, $\left[\boldsymbol{\mathcal{K}}_{(\Gamma_0,\Gamma)}\right]$ and $\left[\boldsymbol{\mathcal{H}}_{(\Gamma_0,\Gamma)}\right]$ that correspond to discrete approximations of the operators in Equations 4-7. Similarly, for $\vec{x}_i \in \Gamma$ the sums in Equation 37 will be reduced to obtain the $N \times N$ complex matrices $\left[\boldsymbol{\mathcal{S}}^{\pm}_{(\Gamma)}\right]$, $\left[\boldsymbol{\mathcal{D}}^{\pm}_{(\Gamma)}\right]$, $\left[\boldsymbol{\mathcal{K}}^{\pm}_{(\Gamma)}\right]$ and $\left[\boldsymbol{\mathcal{H}}^{\pm}_{(\Gamma)}\right]$ that correspond to discrete approximations of the operators in Equations 9-12.

4.1.1 Explicit approach

The discretization of the Dirichlet-to-Neumann $\left[\mathbf{Y}^{\pm}_{(dn,\Gamma)}\right]$ and Neumann-to-Dirichlet $\left[\mathbf{Y}^{\pm}_{(nd,\Gamma)}\right]$ boundary operators gives the matrix equation

$$\mathbf{v}^s = \left[\mathbf{Y}^{\pm}_{(dn,\Gamma)}\right]\mathbf{p}^s, \quad \mathbf{p}^s = \left[\mathbf{Y}^{\pm}_{(nd,\Gamma)}\right]\mathbf{v}^s \tag{47}$$

For the direct formulation we found that

$$\begin{aligned}\left[\mathbf{Y}^{\pm}_{(nd,\Gamma)}\right] &:= i\rho\omega\left(\left[\boldsymbol{\mathcal{D}}^{\pm}_{(\Gamma)}\right] \pm [\mathbf{I}]\right)^{-1}\left[\boldsymbol{\mathcal{S}}^{\pm}_{(\Gamma)}\right], \\ \left[\mathbf{Y}^{\pm}_{(dn,\Gamma)}\right] &:= \frac{1}{i\rho\omega}\left[\boldsymbol{\mathcal{S}}^{\pm}_{(\Gamma)}\right]^{-1}\left(\left[\boldsymbol{\mathcal{D}}^{\pm}_{(\Gamma)}\right] \pm [\mathbf{I}]\right),\end{aligned} \tag{48}$$

where $[\mathbf{I}]$ is the $N \times N$ identity matrix. For the indirect formulation with single source formulation we have the relations

$$\begin{aligned}\left[\mathbf{Y}^{\pm}_{(nd,\Gamma)}\right] &:= i\rho\omega\left[\boldsymbol{\mathcal{S}}^{\pm}_{(\Gamma)}\right]\left[\boldsymbol{\mathcal{K}}^{\pm}_{(\Gamma)}\right]^{-1}, \\ \left[\mathbf{Y}^{\pm}_{(dn,\Gamma)}\right] &:= \frac{1}{i\rho\omega}\left[\boldsymbol{\mathcal{K}}^{\pm}_{(\Gamma)}\right]\left[\boldsymbol{\mathcal{S}}^{\pm}_{(\Gamma)}\right]^{-1},\end{aligned} \tag{49}$$

for the indirect formulation with double source formulation

$$\begin{aligned}\left[\mathbf{Y}^{\pm}_{(nd,\Gamma)}\right] &:= i\rho\omega\left[\boldsymbol{\mathcal{D}}^{\pm}_{(\Gamma)}\right]\left[\boldsymbol{\mathcal{H}}^{\pm}_{(\Gamma)}\right]^{-1}, \\ \left[\mathbf{Y}^{\pm}_{(dn,\Gamma)}\right] &:= \frac{1}{i\rho\omega}\left[\boldsymbol{\mathcal{H}}^{\pm}_{(\Gamma)}\right]\left[\boldsymbol{\mathcal{D}}^{\pm}_{(\Gamma)}\right]^{-1},\end{aligned} \tag{50}$$

and for the indirect formulation with a combination of sources

$$\begin{aligned}\left[\mathbf{Y}^{\pm}_{(nd,\Gamma)}\right] &:= i\rho\omega\left(\left[\boldsymbol{\mathcal{S}}^{\pm}_{(\Gamma)}\right] + i\eta\left[\boldsymbol{\mathcal{D}}^{\pm}_{(\Gamma)}\right]\right)\left(\left[\boldsymbol{\mathcal{K}}^{\pm}_{(\Gamma)}\right] + i\eta\left[\boldsymbol{\mathcal{H}}^{\pm}_{(\Gamma)}\right]\right)^{-1}, \\ \left[\mathbf{Y}^{\pm}_{(dn,\Gamma)}\right] &:= \frac{1}{i\rho\omega}\left(\left[\boldsymbol{\mathcal{K}}^{\pm}_{(\Gamma)}\right] + i\eta\left[\boldsymbol{\mathcal{H}}^{\pm}_{(\Gamma)}\right]\right)\left(\left[\boldsymbol{\mathcal{S}}^{\pm}_{(\Gamma)}\right] + i\eta\left[\boldsymbol{\mathcal{D}}^{\pm}_{(\Gamma)}\right]\right)^{-1}.\end{aligned} \tag{51}$$

The boundary element methods give the discretization of Equations 45 and 46

$$\left[\boldsymbol{\mathcal{G}}^{(d,\pm)}_{(\Gamma_0,\Gamma)}\right]\mathbf{p}^s = \mathbf{p}, \quad \left[\boldsymbol{\mathcal{G}}^{(n,\pm)}_{(\Gamma_0,\Gamma)}\right]\mathbf{v}^s = \mathbf{p}. \tag{52}$$

With the help of the boundary operators $\left[\mathbf{Y}^{\pm}_{(dn,\Gamma)}\right]$, $\left[\mathbf{Y}^{\pm}_{(nd,\Gamma)}\right]$ we can find an explicit representation of the operators $\left[\mathcal{G}^{(d,\pm)}_{(\Gamma_0,\Gamma)}\right]$, $\left[\mathcal{G}^{(n,\pm)}_{(\Gamma_0,\Gamma)}\right]$ for the direct formulations

$$\begin{aligned}\left[\mathcal{G}^{(d,\pm)}_{(\Gamma_0,\Gamma)}\right] &:= \pm\left(i\rho\omega\left[\mathcal{S}_{(\Gamma_0,\Gamma)}\right]\left[\mathbf{Y}^{\pm}_{(nd,\Gamma)}\right]-\left[\mathcal{D}_{(\Gamma_0,\Gamma)}\right]\right),\\ \left[\mathcal{G}^{(n,\pm)}_{(\Gamma_0,\Gamma)}\right] &:= \pm\left(i\rho\omega\left[\mathcal{S}_{(\Gamma_0,\Gamma)}\right]-\left[\mathcal{D}_{(\Gamma_0,\Gamma)}\right]\left[\mathbf{Y}^{\pm}_{(dn,\Gamma)}\right]\right).\end{aligned} \tag{53}$$

The indirect formulations with single source will have the expressions

$$\begin{aligned}\left[\mathcal{G}^{(d,\pm)}_{(\Gamma_0,\Gamma)}\right] &:= \left[\mathcal{S}_{(\Gamma_0,\Gamma)}\right]\left[\mathcal{S}^{\pm}_{(\Gamma)}\right]^{-1},\\ \left[\mathcal{G}^{(n,\pm)}_{(\Gamma_0,\Gamma)}\right] &:= i\rho\omega\left[\mathcal{S}_{(\Gamma_0,\Gamma)}\right]\left[\mathcal{K}^{\pm}_{(\Gamma)}\right]^{-1},\end{aligned} \tag{54}$$

for the double source

$$\begin{aligned}\left[\mathcal{G}^{(d,\pm)}_{(\Gamma_0,\Gamma)}\right] &:= \left[\mathcal{D}_{(\Gamma_0,\Gamma)}\right]\left[\mathcal{D}^{\pm}_{(\Gamma)}\right]^{-1},\\ \left[\mathcal{G}^{(n,\pm)}_{(\Gamma_0,\Gamma)}\right] &:= i\rho\omega\left[\mathcal{D}_{(\Gamma_0,\Gamma)}\right]\left[\mathcal{H}^{\pm}_{(\Gamma)}\right]^{-1},\end{aligned} \tag{55}$$

and for a combination of sources

$$\begin{aligned}\left[\mathcal{G}^{(d,\pm)}_{(\Gamma_0,\Gamma)}\right] &:= \left(\left[\mathcal{S}_{(\Gamma_0,\Gamma)}\right]+i\eta\left[\mathcal{D}_{(\Gamma_0,\Gamma)}\right]\right)\left(\left[\mathcal{S}^{\pm}_{(\Gamma)}\right]+i\eta\left[\mathcal{H}^{\pm}_{(\Gamma)}\right]\right)^{-1},\\ \left[\mathcal{G}^{(n,\pm)}_{(\Gamma_0,\Gamma)}\right] &:= i\rho\omega\left(\left[\mathcal{S}_{(\Gamma_0,\Gamma)}\right]+i\eta\left[\mathcal{D}_{(\Gamma_0,\Gamma)}\right]\right)\left(\left[\mathcal{K}^{\pm}_{(\Gamma)}\right]+i\eta\left[\mathcal{H}^{\pm}_{(\Gamma)}\right]\right)^{-1}.\end{aligned} \tag{56}$$

4.1.2 Implicit approach

Using the boundary element method for the indirect formulation we obtain the equations for the single source

$$\left[\mathcal{S}_{(\Gamma_0,\Gamma)}\right]\boldsymbol{\varphi}=\mathbf{p}, \tag{57}$$

$$\left[\mathcal{S}^{\pm}_{(\Gamma)}\right]\boldsymbol{\varphi}=\mathbf{p}^s,\quad \frac{1}{i\rho\omega}\left[\mathcal{K}^{\pm}_{(\Gamma)}\right]\boldsymbol{\varphi}=\mathbf{v}^s, \tag{58}$$

for the double source

$$\left[\mathcal{D}_{(\Gamma_0,\Gamma)}\right]\boldsymbol{\varphi}=\mathbf{p}, \tag{59}$$

$$\left[\mathcal{D}^{\pm}_{(\Gamma)}\right]\boldsymbol{\varphi}=\mathbf{p}^s,\quad \frac{1}{i\rho\omega}\left[\mathcal{H}^{\pm}_{(\Gamma)}\right]\boldsymbol{\varphi}=\mathbf{v}^s, \tag{60}$$

for a combination of sources

$$\left(\left[\mathcal{S}_{(\Gamma_0,\Gamma)}\right]+i\eta\left[\mathcal{D}_{(\Gamma_0,\Gamma)}\right]\right)\boldsymbol{\varphi}=\mathbf{p}, \tag{61}$$

$$\left(\left[\mathcal{S}^{\pm}_{(\Gamma)}\right]+i\eta\left[\mathcal{D}^{\pm}_{(\Gamma)}\right]\right)\boldsymbol{\varphi}=\mathbf{p}^s,\quad \frac{1}{i\rho\omega}\left(\left[\mathcal{K}^{\pm}_{(\Gamma)}\right]+i\eta\left[\mathcal{H}^{\pm}_{(\Gamma)}\right]\right)\boldsymbol{\varphi}=\mathbf{v}^s, \tag{62}$$

and for the direct approach the system

$$\begin{bmatrix}\mathbf{p}\\ 0\end{bmatrix}=\begin{bmatrix}\pm i\rho\omega\left[\mathcal{S}_{(\Gamma_0,\Gamma)}\right] & \mp\left[\mathcal{D}_{(\Gamma_0,\Gamma)}\right]\\ \pm i\rho\omega\left[\mathcal{S}^{\pm}_{(\Gamma)}\right] & \mp\left(\left[\mathcal{D}^{\pm}_{(\Gamma)}\right]\pm[\mathbf{I}]\right)\end{bmatrix}\begin{bmatrix}\mathbf{v}^s\\ \mathbf{p}^s\end{bmatrix} \tag{63}$$

4.1.3 Modified approach

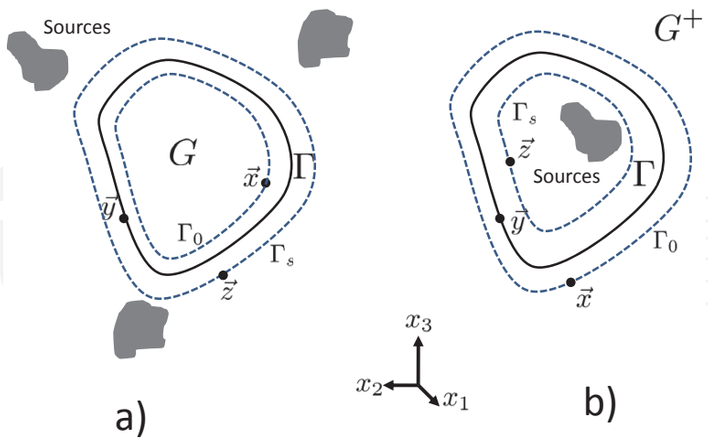


Fig. 5. Boundary setup with source surface for (a) interior NAH and (b) exterior NAH.

One of the major drawbacks of the previous methods is the calculation of the singularity for the matrices $\left[\boldsymbol{\mathcal{S}}\,{}^{\pm}_{(\Gamma)}\right]$,$[\left[\boldsymbol{\mathcal{D}}\,{}^{\pm}_{(\Gamma)}\right]]$, $\left[\boldsymbol{\mathcal{K}}\,{}^{\pm}_{(\Gamma)}\right]$ and $\left[\boldsymbol{\mathcal{H}}\,{}^{\pm}_{(\Gamma)}\right]$. A modified approach requires the definition of a conformal surface Γ_s as in Fig. 4. We construct the $M \times N_s$ complex matrices $\left[\boldsymbol{\mathcal{S}}\,{}_{(\Gamma_0,\Gamma_s)}\right]$,$\left[\boldsymbol{\mathcal{D}}\,{}_{(\Gamma_0,\Gamma_s)}\right]$, $\left[\boldsymbol{\mathcal{K}}\,{}_{(\Gamma_0,\Gamma_s)}\right]$ and $\left[\boldsymbol{\mathcal{H}}\,{}_{(\Gamma_0,\Gamma_s)}\right]$ in the same way as in previous sections, but the integration is over N_s points in the surface Γ_s. Similarly we obtain the $N \times N_s$ complex matrices $\left[\boldsymbol{\mathcal{S}}\,{}_{(\Gamma,\Gamma_s)}\right]$,$\left[\boldsymbol{\mathcal{D}}\,{}_{(\Gamma,\Gamma_s)}\right]$, $\left[\boldsymbol{\mathcal{K}}\,{}_{(\Gamma,\Gamma_s)}\right]$ and $\left[\boldsymbol{\mathcal{H}}\,{}_{(\Gamma,\Gamma_s)}\right]$ that correspond to discrete approximations of the operators in Equations 9-12.
For the indirect formulation we obtain the equations for the single source

$$\left[\boldsymbol{\mathcal{S}}\,{}_{(\Gamma_0,\Gamma_s)}\right]\boldsymbol{\varphi} = \mathbf{p}, \tag{64}$$

$$\left[\boldsymbol{\mathcal{S}}\,{}_{(\Gamma,\Gamma_s)}\right]\boldsymbol{\varphi} = \mathbf{p}^s, \quad \frac{1}{i\rho\omega}\left[\boldsymbol{\mathcal{K}}\,{}_{(\Gamma,\Gamma_s)}\right]\boldsymbol{\varphi} = \mathbf{v}^s, \tag{65}$$

for the double source

$$\left[\boldsymbol{\mathcal{D}}\,{}_{(\Gamma_0,\Gamma_s)}\right]\boldsymbol{\varphi} = \mathbf{p}, \tag{66}$$

$$\left[\boldsymbol{\mathcal{D}}\,{}_{(\Gamma,\Gamma_s)}\right]\boldsymbol{\varphi} = \mathbf{p}^s, \quad \frac{1}{i\rho\omega}\left[\boldsymbol{\mathcal{H}}\,{}_{(\Gamma,\Gamma_s)}\right]\boldsymbol{\varphi} = \mathbf{v}^s, \tag{67}$$

and for a combination of sources

$$\left(\left[\boldsymbol{\mathcal{S}}\,{}_{(\Gamma_0,\Gamma_s)}\right] + i\eta\left[\boldsymbol{\mathcal{D}}\,{}_{(\Gamma_0,\Gamma_s)}\right]\right)\boldsymbol{\varphi} = \mathbf{p}, \tag{68}$$

$$\left(\left[\boldsymbol{\mathcal{S}}\,{}_{(\Gamma,\Gamma_s)}\right] + i\eta\left[\boldsymbol{\mathcal{D}}\,{}_{(\Gamma,\Gamma_s)}\right]\right)\boldsymbol{\varphi} = \mathbf{p}^s, \quad \frac{1}{i\rho\omega}\left(\left[\boldsymbol{\mathcal{D}}\,{}_{(\Gamma,\Gamma_s)}\right] + i\eta\left[\boldsymbol{\mathcal{H}}\,{}_{(\Gamma,\Gamma_s)}\right]\right)\boldsymbol{\varphi} = \mathbf{v}^s. \tag{69}$$

4.2 Equivalent sources method

The equivalent sources method can be understood as an approximation of the boundary element method modified approach. For $\vec{x}_i, i = 1, ..., M$, in Γ_0 and $\vec{z}_i, i = 1, ..., N_s$ in Γ_s we

obtain the matrix approximations of $\left[\boldsymbol{S}_{(\Gamma,\Gamma_s)}\right]$,$\left[\boldsymbol{D}_{(\Gamma,\Gamma_s)}\right]$, $\left[\boldsymbol{K}_{(\Gamma,\Gamma_s)}\right]$ and $\left[\boldsymbol{H}_{(\Gamma,\Gamma_s)}\right]$ given by Equation 41-44. There

$$\left[\boldsymbol{S}_{(\Gamma_0,\Gamma_s)}\right]\mathbf{q}=\mathbf{p}, \tag{70}$$

$$\left[\boldsymbol{S}_{(\Gamma,\Gamma_s)}\right]\mathbf{q}=\mathbf{p}^s,\quad \frac{1}{i\rho\omega}\left[\boldsymbol{K}_{(\Gamma,\Gamma_s)}\right]\mathbf{q}=\mathbf{v}^s, \tag{71}$$

for the double source

$$\left[\boldsymbol{D}_{(\Gamma_0,\Gamma_s)}\right]\mathbf{q}=\mathbf{p}, \tag{72}$$

$$\left[\boldsymbol{D}_{(\Gamma,\Gamma_s)}\right]\mathbf{q}=\mathbf{p}^s,\quad \frac{1}{i\rho\omega}\left[\boldsymbol{H}_{(\Gamma,\Gamma_s)}\right]\mathbf{q}=\mathbf{v}^s, \tag{73}$$

and for a combination of sources

$$\left(\left[\boldsymbol{S}_{(\Gamma_0,\Gamma_s)}\right]+i\eta\left[\boldsymbol{D}_{(\Gamma_0,\Gamma_s)}\right]\right)\mathbf{q}=\mathbf{p}, \tag{74}$$

$$\left(\left[\boldsymbol{S}_{(\Gamma,\Gamma_s)}\right]+i\eta\left[\boldsymbol{D}_{(\Gamma,\Gamma_s)}\right]\right)\mathbf{q}=\mathbf{p}^s,\quad \frac{1}{i\rho\omega}\left(\left[\boldsymbol{K}_{(\Gamma,\Gamma_s)}\right]+i\eta\left[\boldsymbol{H}_{(\Gamma,\Gamma_s)}\right]\right)\mathbf{q}=\mathbf{v}^s. \tag{75}$$

5. Numerical regularization

For the experimental problem, the exact pressure $\mathbf{p}$ is perturbed by measurement errors. We denote the measured pressure as $\widetilde{\mathbf{p}}$. If the elements of the perturbation $\mathbf{e}=\widetilde{\mathbf{p}}-\mathbf{p}$ are Gaussian (unbiased and uncorrelated) with covariance matrix $\sigma_0^2\,[\mathbf{I}]$, then $E\left(\|\mathbf{e}\|_2^2\right)=M\sigma_0^2$, where $\|.\|_2$ is the 2-norm. It is well known that the linear systems in Equation 52, Equations 57,59,61,63, Equations 64, 66,68, and Equations 70, 72,74, are ill-posed, i.e., the errors in $\widetilde{\mathbf{p}}$ will be amplified on the solutions $\mathbf{p}^s$, $\mathbf{v}^s$, $\boldsymbol{\varphi}$ or $\mathbf{q}$ and in most of the cases the recovery will be useless.
Consider the solution of the generic ill-posed linear matrix system

$$[\mathbf{A}]\,\mathbf{z}=\widetilde{\mathbf{p}}. \tag{76}$$

Here $[\mathbf{A}]$, $\mathbf{z}$, $\widetilde{\mathbf{p}}$ represent the ill-posed matrix, the solution of the linear system and the measurement vector of Equations 52,57,59, 61,63, 64, 66, 68, 70, 72, and 74. Let $\overline{M}\times\overline{N}$ be the dimension of the matrix $[\mathbf{A}]$. Then $\mathbf{z}$, $\widetilde{\mathbf{P}}$ are column vectors of $\overline{N}$, $\overline{M}$ entries respectively. For Equations 52,57,59, and 61, $\overline{M}=M$ and $\overline{N}=N$. For Equation 63, $\overline{M}=2M$ and $\overline{N}=2N$. For Equations 64,66,68, 70, 72, and 74, $\overline{M}=M$ and $\overline{N}=N_s$. The ill-posedness of the matrix system Equation 76 can be explained using the singular value decomposition (SVD)

$$[\mathbf{A}]=[\mathbf{U}][\mathbf{\Sigma}][\mathbf{V}]^H$$

where $[\mathbf{U}]$ and $[\mathbf{V}]$ are unitary matrices of dimension $\overline{M}\times\overline{M}$ and $\overline{N}\times\overline{N}$, respectively, and $[\mathbf{V}]^H$ is the conjugate transpose of $[\mathbf{V}]$. $[\mathbf{\Sigma}]=$ is a diagonal matrix with values $\sigma_1\geq\ldots\geq\sigma_{N^*}\geq 0$ where $N^*=\text{rank}\,([\mathbf{A}])$. The values σ_i are called the singular values.
Denote $\mathbf{u}_i$, $i=1,\ldots,M$ and $\mathbf{v}_i$, $i=1,\ldots,N$, the columns of $[\mathbf{U}]$ and $[\mathbf{V}]$ respectively. For NAH, $\mathbf{u}_i$, $\mathbf{v}_i$ will be an approximation to the acoustic field by basic acoustic waves or *mode shapes* (see Williams et al. (2000)). In particular when $[\mathbf{A}]=\left[\boldsymbol{\mathcal{G}}_{(\Gamma_0,\Gamma)}^{(n,\pm)}\right]$ (as in Equation 52), $\mathbf{u}_i$ will be the modes of the measured pressure on Γ_0 and $\mathbf{v}_i$ will be the modes of the normal velocity

on Γ. These modes are organized in such a way that the first modes are related with the non-evanescent waves and the last modes will be related with the evanescent waves.
The solution to Equation 76 by conventional methods can be explicitly written as

$$\mathbf{z}_{LS} = \sum_{i=1}^{N^*} \frac{\left(\mathbf{u}_i^H \widetilde{\mathbf{p}}\right)}{\sigma_i} \mathbf{v}_i. \tag{77}$$

Notice that this solution will include modes $\mathbf{u}_i$, $\mathbf{v}_i$ that are related to both non-evanescent and evanescent waves. It is well known that the modes related to the evanescent waves will produce the fine details of the reconstruction $\mathbf{z}_{LS}$, but at the same time will amplify the noise in $\widetilde{\mathbf{p}}$. Regularization methods for the solution to this inverse acoustic problem will need to include enough of these modes in order to obtain the desired resolution, and at the same time exclude some of these modes that are totally corrupted with noise.
As explained in Hansen (1998), regularization methods for the solution $\mathbf{z}$ of Equation 76 can be distinguished as *direct* and *iterative*.

5.1 Direct regularization

For the direct regularization the solution of Equation 76 is written explicitly with the help of the SVD as

$$\mathbf{z}_\alpha = \sum_{i=1}^{N^*} f_i^\alpha \left(\frac{\mathbf{u}_i^H \widetilde{\mathbf{p}}}{\sigma_i} \right) \mathbf{v}_i, \tag{78}$$

where α is the regularization parameter and f_i^α, $i = 1, ..., N^*$ are the *filter factors* (see Engl et al. (1996); Hansen (1998)). The parameter α will control the inclusion of modes related to evanescent waves into the solution $\mathbf{z}_\alpha$. The topic of direct regularization methods for linear matrix systems has been extensively studied in the last few decades. The best known regularization approach is the classical Tikhonov regularization, but there are many other approaches depending on the particular problem like damped SVD, truncated SVD or Tikhonov with High-pass filter. These approaches are defined by their respective filters

$$f^{(1,\alpha_i)} = \frac{\sigma_i^2}{\sigma_i^2 + \alpha^2}, \quad f^{(2,\alpha_i)} = \frac{\sigma_i}{\sigma_i + \alpha}, \quad f^{(3,\alpha_i)} = \begin{cases} 1, i \leq \alpha \\ 0, i > \alpha \end{cases}, \quad f^{(4,\alpha_i)} = \frac{\sigma_i^2}{\sigma_i^2 + \alpha^2 \left(\frac{\alpha^2}{\alpha^2 + \sigma_i^2} \right)}.$$

Tikhonov regularization with a high-pass filter (see Williams (2001)) uses the physical behavior of the evanescent waves to produce an optimal filter.

5.2 Iterative methods

Iterative regularization methods for the linear system Equation 76 are based on iteration schemes that access the coefficient matrix $[\mathbf{A}]$ only via matrix-vector multiplications with $[\mathbf{A}]$ and $[\mathbf{A}]^H$. They produce a sequence of iteration vectors $\mathbf{z}_{(l)}$, $l = 1, 2, 3, ...$, that converge to $\vec{z}_{LS}$ in Equation 78. For ill-posed linear systems these methods produce the phenomena of "semi-convergence", i.e., the vector $\mathbf{z}_{(l)}$ approaches the optimal regularization solution after a few iterations l. If the iteration is not stopped, the method converges to the least squares solution $\mathbf{z}_{LS}$ in Equation 78 which is generally totally corrupted by the noisy data $\widetilde{\mathbf{p}}$. In this case each iteration vector $\mathbf{z}_{(l)}$ can be considered as a regularized solution, with the iteration number l playing the role of the regularization parameter. These iterative methods are preferable to direct methods when the matrix $[\mathbf{A}]$ is so large that it is too time consuming or too memory-demanding to work with the SVD of $[\mathbf{A}]$. In the next section we will discuss a special type of iterative methods named Krylov subspace methods.

starting vector $\mathbf{z}_{(0)} = 0$
$\mathbf{r}_{(0)} = \widetilde{\mathbf{p}}$
$\mathbf{d}_{(0)} = [\mathbf{A}]^H \mathbf{r}_{(0)}$
for $l = 1, 2, \ldots (\leq \min(M, N))$
$\alpha_{(l)} = \left\| [\mathbf{A}]^H \mathbf{r}_{(l-1)} \right\|_2^2 / \left\| [\mathbf{A}] \mathbf{d}_{(l-1)} \right\|_2^2,$
$\mathbf{z}_{(l)} = \mathbf{z}_{(l-1)} + \alpha_{(l)} \mathbf{d}_{(l-1)},$
$\mathbf{r}_{(l)} = \mathbf{r}_{(l-1)} - \alpha_{(l)} [\mathbf{A}] \mathbf{d}_{(l-1)}$
$\beta_{(l)} = \left\| [\mathbf{A}]^H \mathbf{r}_{(l)} \right\|_2^2 / \left\| [\mathbf{A}]^H \mathbf{r}_{(l-1)} \right\|_2^2,$
$\mathbf{d}_{(l)} = [\mathbf{A}]^H \mathbf{r}_{(l)} + \beta_{(l)} \mathbf{d}_{(l-1)},$

Table 3. Algorithm for Conjugate Gradients for the Normal Equations.

initial step
$\mathbf{z}_{(0)} = 0$
$\beta_{(1)} \mathbf{u}_{(1)} = \widetilde{\mathbf{p}}, \quad \alpha_{(1)} \mathbf{v}_{(1)} = [\mathbf{A}]^H \mathbf{u}_{(1)}$
$\mathbf{w}_{(1)} = \mathbf{v}_{(1)}, \quad \overline{\phi}_{(1)} = \beta_{(1)}, \overline{\rho}_{(1)} = \alpha_{(1)}$
for $l = 1, 2, \ldots (\leq N^*)$
$\mathbf{p} = [\mathbf{A}] \mathbf{v}_{(l)} - \alpha_{(l)} \mathbf{u}_{(l)}$
for $j = 1, \ldots, (l-1)$
$\mathbf{p} = \mathbf{p} - \left(\mathbf{u}_{(j)}^H \mathbf{p} \right) \mathbf{u}_{(j)}$
} (Reorthogonalization)
$\beta_{(l+1)} \mathbf{u}_{(l+1)} = \mathbf{p}$
$\mathbf{r} = [\mathbf{A}]^H \mathbf{u}_{(l)} - \beta_{(l)} \mathbf{v}_{(l-1)}$
for $j = 1, \ldots, (l-1)$
$\mathbf{r} = \mathbf{r} - \left(\mathbf{v}_{(j)}^H \mathbf{r} \right) \mathbf{v}_{(j)}$
} (Reorthogonalization)
$\alpha_{(l+1)} \mathbf{v}_{(l+1)} = \mathbf{r}_{(l)}$
$\rho_{(l)} = \sqrt{(\overline{\rho}_{(l)})^2 + \beta_{(l+1)}^2}$
$c_{(l)} = \overline{\rho}_{(l)} / \rho_{(l)} \quad s_{(l)} = \beta_{(l+1)} / \rho_{(l)}$
} (Givens Rotations)
$\theta_{(l+1)} = s_{(l)} \alpha_{(l+1)}, \quad \overline{\rho}_{(l+1)} = c_{(l)} \alpha_{(l+1)}$
$\phi_{(l+1)} = c_{(l)} \overline{\phi}_{(l)}, \quad \overline{\phi}_{(l+1)} = -s_{(l)} \overline{\phi}_{(l)}$
$\mathbf{z}_{(l)} = \mathbf{z}_{(l-1)} + \left(\frac{\phi_{(l)}}{\rho_{(l)}} \right) \mathbf{w}_{(l)}$
$\mathbf{w}_{(l+1)} = \mathbf{v}_{(l+1)} - \left(\frac{\theta_{(l+1)}}{\rho_{(l)}} \right) \mathbf{w}_{(l)}$

Table 4. Algorithm for LSQR.

5.2.1 Krylov subpace iterative methods

This section presents some general features of the Krylov subspace methods, and focuses on two of these methods: conjugate gradients for the normal equations (CGNE) (see Table 3) and

least squares QR (LSQR) (see Table 4). Consider the normal equations of Equation 76,

$$[\mathbf{A}]^H [\mathbf{A}] \mathbf{z} = [\mathbf{A}]^H \widetilde{\mathbf{p}}. \tag{79}$$

The solution to Equation 79 is equal to the least squares solution $\mathbf{z}_{LS}$ given in Equation 78. The CGNE iterative algorithm (given in Table 3) produces, for each iteration l, the vector $\mathbf{z}_{(l)}$ that approximates the least squares solution $\mathbf{z}_{LS}$ to Equation 79. Notice from Table 3, line 6, that on iteration $l = 1$ of CGNE, $\mathbf{z}_{(1)}$ is formed by the vector $[\mathbf{A}]^H \widetilde{\mathbf{p}}$ multiplied by a constant. On iteration $l = 2$, $\mathbf{z}_{(2)}$ is formed by $c_1 [\mathbf{A}]^H \widetilde{\mathbf{p}} + c_2 \left([\mathbf{A}]^H [\mathbf{A}] \right) [\mathbf{A}]^H \widetilde{\mathbf{p}}$, where c_1, c_2 are constants. Similarly, for each l, a vector $\mathbf{z}_{(l)}$ can be expressed as

$$\mathbf{z}_{(l)} = \sum_{i=0}^{l-1} c_i \left([\mathbf{A}]^H [\mathbf{A}] \right)^i [\mathbf{A}]^H \widetilde{\mathbf{p}}, \tag{80}$$

where c_i, $i = 0, ..., l-1$ are constants. In mathematical notation, this combination of vectors is called the *Krylov subspace* l, and is denoted as $\mathcal{K}^{(l)} \left([\mathbf{A}]^H \widetilde{\mathbf{p}}, [\mathbf{A}]^H [\mathbf{A}] \right)$. We write, instead of Equation 80, $\mathbf{z}_{(l)} \in \mathcal{K}^{(l)} \left([\mathbf{A}]^H \widetilde{\mathbf{p}}, [\mathbf{A}]^H [\mathbf{A}] \right)$. There are a variety of iterative methods that, for each iteration l, produce vectors $\mathbf{z}_{(l)}$ that belong to the Krylov subspace l (at each iteration $\mathbf{z}_{(l)}$ can be written as Equation 80). For that reason these methods are called *Krylov Subspace methods* (see Hanke (1995)). It is not obvious, but it can be shown that in general the Krylov subspace methods will approximate the least squares solution $\mathbf{z}_{LS}$ to Equation 79 as l increases (see Hanke (1995), Valdivia & Williams (2005)). CGNE is the most representative Krylov subspace method for the solution to the normal equations in Equation 79. There is also a wide variety of well known Krylov subspace methods like Landweber or Generalized Minimal Residual (GMRES) (see Hanke (1995) for more information). When the matrix $[\mathbf{A}]$ in Equation 76 is square (the dimensions $M = N$) then Krylov subspace methods like GMRES are more commonly used. These methods are based directly in the solution to Equation 76 where $\mathbf{z}_{(l)} \in \mathcal{K}^{(l)} (\widetilde{\mathbf{p}}, [\mathbf{A}])$ (see Calvetti et al. (2001a;b; 2002)).
Despite the simplicity of the CGNE algorithm, each iterate $\mathbf{z}_{(l)}$ satisfies

$$\| [\mathbf{A}] \mathbf{z}_{(l)} - \widetilde{\mathbf{p}} \|_2 \leq \| [\mathbf{A}] \mathbf{h} - \widetilde{\mathbf{p}} \|_2, \tag{81}$$

for all vectors $\mathbf{h} \in \mathcal{K}^{(l)} \left([\mathbf{A}]^H \widetilde{\mathbf{p}}, [\mathbf{A}]^H [\mathbf{A}] \right)$. Another important property of the CGNE algorithm is that

$$\| [\mathbf{A}] \mathbf{z}_{(l)} - \widetilde{\mathbf{p}} \|_2 \leq \| [\mathbf{A}] \mathbf{z}_{(l-1)} - \widetilde{\mathbf{p}} \|_2, \quad \| \mathbf{z}_{(l-1)} \|_2 \leq \| \mathbf{z}_{(l)} \|_2. \tag{82}$$

The proof of these properties is rather technical, so we recommend references Engl et al. (1996); Hanke (1995) for more details.

5.3 Regularization parameter choice methods

We utilize the following definition for our presentation of parameter choice

$$\mathbf{z} = [\mathbf{A}]^\dagger \mathbf{p}, \quad \mathbf{z}_\alpha = [\mathbf{A}]^\# \widetilde{\mathbf{p}}$$

where $[\mathbf{A}]^\dagger = \left([\mathbf{A}]^H [\mathbf{A}] \right)^{-1} [\mathbf{A}]^H$ is the generalized inverse and $[\mathbf{A}]^\#$ is the operator of the regularization method.

The most widespread parameter choice method is the discrepancy principle, usually attributed to Morozov. This method is based on a good estimation of the error $\|\mathbf{e}\| = \delta_e$ so we solve the problem

$$\| [\mathbf{A}]\, \mathbf{z}_\alpha - \widetilde{\mathbf{p}}\|_2 = \delta_e, \tag{83}$$

for a parameter α.
There are very successful methods that do not depend on the estimation of noise. Two of the most successful methods are Generalized Cross-Validation (GCV) and the L-curve analysis. In GCV we define the function

$$\mathcal{G}(\alpha) = \frac{\| [\mathbf{A}]\, \mathbf{z}_\alpha - \widetilde{\mathbf{p}}\|_2^2}{\text{trace}\left([\mathbf{I}] - [\mathbf{A}]\, [\mathbf{A}]^{\#}\right)^2}, \tag{84}$$

and the optimal regularization parameter α is the parameter that is the minimum of the function $\mathcal{G}$.
In the L-curve analysis we define the parametric curve $(x(\alpha), y(\alpha)$ where

$$x(\alpha) = \log \| [\mathbf{A}]\, \mathbf{z}_\alpha - \widetilde{\mathbf{p}}\|_2, \quad y(\alpha) = \log \|\mathbf{z}_\alpha\|_2,$$

and the optimal parameter will be the point α where the curvature

$$\kappa(\alpha) = \frac{x'y'' - x''y'}{((x')^2 + (y')^2)^{3/2}} \tag{85}$$

attains its maximum. Here the differentiation $'$ is with respect to α.

5.3.1 Direct regularization

For direct regularization we utilize the following simplifications that come from the SVD, to obtain

$$\begin{aligned}
\| [\mathbf{A}]\, \mathbf{z}_\alpha - \widetilde{\mathbf{p}}\|_2^2 &= \sum_{i=1}^{N^*} (f_i^{j,\alpha} - 1)^2 |\mathbf{u}_i^H \widetilde{\mathbf{p}}|^2, \\
\text{trace}\left([\mathbf{I}] - [\mathbf{A}]\, [\mathbf{A}]^{\#}\right) &= \overline{M} - \sum_{i=1}^{N^*} f_i^{j,\alpha}, \\
\|\mathbf{z}_\alpha\|_2^2 &= \sum_{i=1}^{N^*} f^{j,\alpha} \frac{|\mathbf{u}_i^H \widetilde{\mathbf{p}}|^2}{\sigma_i^2},
\end{aligned}$$

where the filter factors $f_i^{j,\alpha}$ describe the direct regularization methods defined previously. The GCV and L-curve can be applied directly using the above formulae.
For the Morozov's discrepancy principle in acoustics it was proposed that the error $\|\mathbf{e}\|_2$ be estimated in the following manner. We can define the SNR dB level of tolerance T of our measurements, that under laboratory controlled conditions we can expect $T = -40$ dB. Define the decreasing function $\gamma_i = 20 \log_{10}(\sigma_i/\sigma_1)$ and we denote as i' the index where $\gamma_i < T$, for $i > i'$. Then σ_0 can be approximated by the mean value of the coefficients $|\mathbf{u}_i^H \widetilde{\mathbf{p}}|$ for $i > i'$. This gives the estimate

$$\|\mathbf{e}\|_2 \approx \frac{\sqrt{\overline{\overline{M}}}}{N^* - i' + 1} \sum_{i=i'}^{N^*} |\mathbf{u}_i^H \widetilde{\mathbf{p}}|. \tag{86}$$

5.3.2 Iterative regularization

For iterative methods like CGLS and LSQR if there is a good approximation of δ_e, then in the discrepancy principle, the method will iterate while

$$\| [\mathbf{A}]\, \mathbf{z}_{(l)} - \widetilde{\mathbf{p}} \|_2 \leq \delta_e. \tag{87}$$

To apply GCV (as suggested in Hansen (1998)), we use the approximation to the function $\mathcal{G}$

$$\mathcal{G}(l) = \frac{\| [\mathbf{A}]\, \mathbf{z}_{(l)} - \widetilde{\mathbf{p}} \|_2^2}{(M-l)^2}. \tag{88}$$

For L-curve Hansen & O'Leary (1993), we plot the coordinates

$$x(l) = \log\left(\| [\mathbf{A}]\, \mathbf{z}_{(l)} - \widetilde{\mathbf{p}} \|_2 \right), \quad y(l) = \log\left(\| \vec{z}_{(l)} \|_2 \right), \tag{89}$$

which gives a curve that resembles an L-shape. The optimal iteration l_{opt} is the iteration with coordinates $(x(l_{opt}), y(l_{opt}))$ which are closer to the point of maximum curvature of the L-shaped curve.
Finally we discuss the rule designed by Hanke and Raus Hanke & Raus (1996). In the CGNE algorithm (Table 3) or LSQR algorithm (Table 4), for iteration l we include the sequence

$$\gamma_{(l)} = \left(\frac{\alpha_{(l)} \beta_{(l-1)}}{\alpha_{(l-1)}} + 1 \right) \gamma_{(l-1)} - \left(\frac{\alpha_{(l)} \beta_{(l-1)}}{\alpha_{(l-1)}} \right) \gamma_{(l-2)} + \alpha_{(l)}, \tag{90}$$

where $\gamma_{(0)} = \gamma_{(-1)} = 0$. The optimal iteration l_{opt} is the iteration for which the function

$$\mathcal{H}(l) = |\gamma_{(l)}|^{1/2} \| \vec{r}_{(l)} \|_2, \tag{91}$$

has its minimum value.

6. Numerical examples

In this section we use numerically generated data to help explain some of the numerical difficulties involved in the NAH technique. Here Γ, Γ_0 and the source surface Γ_s are spherical surfaces. Let the acoustic constants in air be denoted as $c = 343 m/s$ and $\rho = 1.21 kg/m^3$. The wave-length given in units of m is defined as $\lambda := c/f$.
We consider the problem of recovering the acoustic field on the surface Γ from pressure measurements on Γ_0. The acoustic field is generated at a point $\vec{x} \in \mathbb{R}^3$ for a dipole using the formula in Williams (1999)

$$\begin{cases} p(\vec{x}) = i\rho\omega Q \left\{ \vec{\alpha} \cdot \nabla \Phi(\vec{x}, \vec{z}) \right\} \\ v(\vec{x}) = Q \frac{\partial}{\partial \vec{n}(\vec{x})} \left\{ \vec{\alpha} \cdot \nabla \Phi(\vec{x}, \vec{z}) \right\} \end{cases} \tag{92}$$

where Q is the source strength with m^3/s units, $\vec{z}$ is the source location and unit direction $\vec{\alpha} = (\alpha_1, \alpha_2, \alpha_3)$. We denote as $\mathbf{p}$ the complex column vector of M entries, where each entry corresponds to a point $p(\vec{x}_i)$ where $\vec{x}_i \in \Gamma_0$. Similarly we denote as $\mathbf{p}^s$, $\mathbf{v}^s$ the complex column vectors of N entries where each entry corresponds to a point $p(\vec{x}_j)$, $v(\vec{x}_j)$, $\vec{x}_j \in \Gamma$. We compute $\widetilde{\mathbf{p}} = \mathbf{p} + \mathbf{e}$ where

$$\mathbf{e} = \left(10^{-D/20} \|\mathbf{p}\|_2 / \sqrt{M} \right) \mathbf{e}_u,$$

where $\mathbf{e}_u$ is the column vector with Gaussian entries (with normal distribution) and D the signal-to-noise ratio (SNR) used to simulate measurement errors.
The Fourier theory suggests that the maximum distance between adjacent points in the discretization of any of the surfaces Γ_0, Γ, Γ_s for a frequency f needs to be less than $\lambda/4$ to avoid any aliasing problem.
We quantify the numerical error in our reconstructions using the relative errors

$$\|\mathbf{p}^s - \mathbf{p}_r^s\|/\|\mathbf{p}^s\| \times 100\% \quad \text{or} \quad \|\mathbf{v}^s - \mathbf{v}_r^s\|/\|\mathbf{v}^s\| \times 100\%$$

where $\mathbf{p}_r^s$,$\mathbf{v}_r^s$ are the pressure and normal velocity fields reconstructed using our NAH schemes described in previous sections.

6.1 Boundary element methods

For BEM the distance between adjacent points in an element should be less than $\lambda/10$ to avoid aliasing problems and guarantee a proper integration over the element. We consider as Γ the unit sphere with the following discretization points

$$\vec{x_1} = (0,0,1), \quad \vec{x_2} = (1,0,0), \quad \vec{x_3} = (0,1,0)$$
$$\vec{x_4} = (-1,0,0), \quad \vec{x_5} = (0,-1,0), \quad \vec{x_6} = (0,0,-1)$$

and triangular elements

$$\triangle_1 = [\vec{x_1},\vec{x_2},\vec{x_3}], \quad \triangle_2 = [\vec{x_1},\vec{x_3},\vec{x_4}], \quad \triangle_3 = [\vec{x_1},\vec{x_4},\vec{x_5}], \quad \triangle_4 = [\vec{x_1},\vec{x_5},\vec{x_2}]$$
$$\triangle_5 = [\vec{x_6},\vec{x_3},\vec{x_2}], \quad \triangle_6 = [\vec{x_6},\vec{x_4},\vec{x_3}], \quad \triangle_7 = [\vec{x_6},\vec{x_5},\vec{x_4}], \quad \triangle_8 = [\vec{x_6},\vec{x_2},\vec{x_5}].$$

The surface Γ_0 will have the same point distribution as Γ, but Γ_0 will be a sphere of radius 1.1 m.

6.1.1 Higher order elements

At $f = 100$ Hz the wavelength $\lambda = 3.43$ m, and $\lambda/10 = 34.3$ cm. We refine our initial triangular discretization $\triangle_1,...,\triangle_8$ using the quadratic element scheme shown in Fig. 2a). The first refinement will produce 18 points and 24 linear triangular elements and 6 quadratic triangular elements. In Table 5 we show the relative error for the reconstruction of the pressure $\mathbf{p}$ in Γ_0 and pressure $\mathbf{p}^s$ in Γ that results from a dipole with position $\vec{z} = (0,0,0.7)$ and direction $\vec{\alpha} = (1/\sqrt{3}, 1/\sqrt{3}, 1/\sqrt{3})$ (given in Equation 92), using the direct formulation

$$\mathbf{p}_r = i\rho\omega \left[\boldsymbol{\mathcal{S}}_{(\Gamma_0,\Gamma)}\right] \mathbf{p}^s - \left[\boldsymbol{\mathcal{D}}_{(\Gamma_0,\Gamma)}\right] \mathbf{v}^s, \quad \mathbf{p}_r^s = i\rho\omega \left[\boldsymbol{\mathcal{S}}^{+}_{(\Gamma)}\right] \mathbf{p}^s - \left[\boldsymbol{\mathcal{D}}^{+}_{(\Gamma)}\right] \mathbf{v}^s,$$

for successive refinements. Each refinement reduces the maximum element diameter by half each time. Notice that the recovery of $\mathbf{p}$ utilizes the non-singular matrices $\left[\boldsymbol{\mathcal{S}}_{(\Gamma_0,\Gamma)}\right]$, $\left[\boldsymbol{\mathcal{D}}_{(\Gamma_0,\Gamma)}\right]$ and the recovery of $\mathbf{p}^s$ utilizes the singular matrices $\left[\boldsymbol{\mathcal{S}}^{+}_{(\Gamma)}\right]$ and $\left[\boldsymbol{\mathcal{D}}^{+}_{(\Gamma)}\right]$.
In Table 5 the order refers to the ratio between refinement errors. In the theory found in the book of Atkinson (1997) this ratio is 2^h, where h is the order. The theory also states that linear elements for a smooth surface like a sphere will have $h = 1$, quadratic elements $h = 2$ and cubic elements $h = 3$. The results in Table 5 show that in practice this order can be higher, and this has always been the major motivation for the use of higher order elements for accurate solutions of the forward problem. The use of higher order element will not be a good idea

	linear		quadratic	
N	Non-singular(order)	Singular(order)	Non-singular(order)	Singular(order)
18	57.5929	42.7929	39.6083	30.3930
66	17.6444(3.2641)	12.7465(3.3572)	29.2035(1.3563)	22.1742(1.3707)
258	7.5391(2.3404)	5.6551(2.2540)	4.7439(6.1560)	4.5844(4.8368)
1026	2.0327(3.7089)	1.5385(3.6757)	0.2107(22.5112)	0.8449(5.4260)

Table 5. relative error comparison for linear and quadratic elements

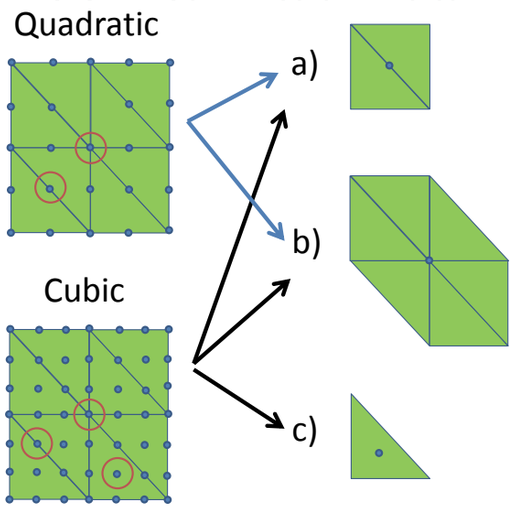


Fig. 6. Triangular decomposition for quadratic and cubic elements. a) multiple triangle intersection for vertex nodes, b) simple edge intersection and c) interior triangle point.

for the inverse problem, where increasing the resolution will pay the penalty of reducing the smoothness of the solution, as we will show.
Let the quantities $W_{m,j}$, $m = 1, ..., n_q$,

$$W_{m,j} = \int_0^1 \int_0^{1-\xi_2} N_m(\xi_1, \xi_2) J(\xi_1, \xi_2) d\xi_1 d\xi_2,$$

for the triangular elements shape functions given in Table 3. These quantities can be thought as approximations of $\mathcal{S}^i_{(m,j)}$, $\mathcal{D}^i_{(m,j)}$, $\mathcal{K}^i_{(m,j)}$, $\mathcal{H}^i_{(m,j)}$ when the field point $\vec{x}_i$ is far from the element $\triangle_j$. We can consider $W_{m,j}$ as an estimate of the column normalized weights (CNW) for the matrices $\left[\boldsymbol{\mathcal{S}}_{(\Gamma_0,\Gamma)}\right]$, $\left[\boldsymbol{\mathcal{D}}_{(\Gamma_0,\Gamma)}\right]$, $\left[\boldsymbol{\mathcal{K}}_{(\Gamma_0,\Gamma)}\right]$ and $\left[\boldsymbol{\mathcal{H}}_{(\Gamma_0,\Gamma)}\right]$.
The following explanation of the CNW will be given for the matrix $\left[\boldsymbol{\mathcal{S}}_{(\Gamma_0,\Gamma)}\right]$, but will also apply to $\left[\boldsymbol{\mathcal{D}}_{(\Gamma_0,\Gamma)}\right]$, $\left[\boldsymbol{\mathcal{K}}_{(\Gamma_0,\Gamma)}\right]$ and $\left[\boldsymbol{\mathcal{H}}_{(\Gamma_0,\Gamma)}\right]$. Notice that $\left[\boldsymbol{\mathcal{S}}_{(\Gamma_0,\Gamma)}\right]$ is obtained by a reduction of the sum $\mathcal{S}^i_{(m,j)}$ and this reduction depends on the triangular elements decomposition used for the surface Γ. Fig. 6 shows quadratic and cubic triangular elements. Observe that the case shown in Fig. 6b) is when a point is intersected by six triangles. This means that when the sum of the quantities $\mathcal{S}^i_{(m,j)}$ are reduced into a column of the matrix $\left[\boldsymbol{\mathcal{S}}_{(\Gamma_0,\Gamma)}\right]$, this point will be associated with the CNW of 6. Using the same argument for the case in Fig. 6a) a column of the matrix $\left[\boldsymbol{\mathcal{S}}_{(\Gamma_0,\Gamma)}\right]$ that corresponds to this point will be associated with the CNW of 2.

Finally, in the case of Fig. 6c), a column of the matrix $\left[\boldsymbol{\mathcal{S}}_{(\Gamma_0,\Gamma)}\right]$ that corresponds to this point will be associated with the CNW of 1. As a result when cubic elements are used, the columns of matrix $\left[\boldsymbol{\mathcal{S}}_{(\Gamma_0,\Gamma)}\right]$ associated with interior points like Fig. 6c will have a CNW of 1. Cubic and quadratic elements for edge points like Fig. 6a) will have a CNW of 2. All elements will have a CNW of 6 in the vertex points.

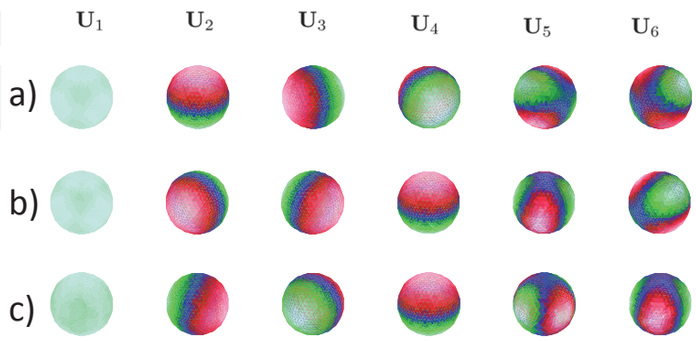


Fig. 7. Plot of the first columns of $[\mathbf{U}]$ from the SVD of $\left[\boldsymbol{\mathcal{S}}_{(\Gamma_0,\Gamma)}\right]$ at $f = 100$ Hz. a) linear elements, b) quadratic elements, and c) cubic elements.

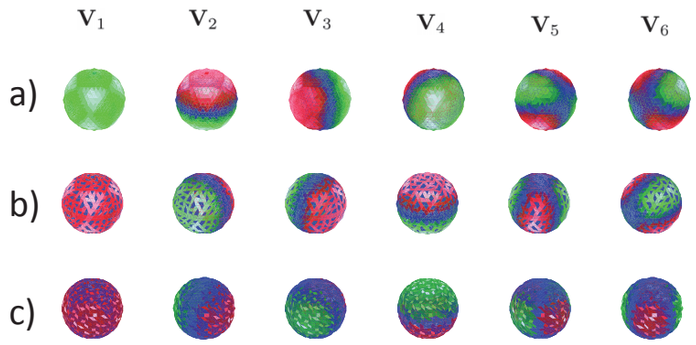


Fig. 8. Plot of the first columns of $[\mathbf{U}]$ from the SVD of $\left[\boldsymbol{\mathcal{S}}_{(\Gamma_0,\Gamma)}\right]$ at $f = 100$ Hz. a) linear elements, b) quadratic elements, and c) cubic elements.

For the reasons exposed in the paragraph above, linear elements will have a constant CNW while quadratic and cubic elements will have an imbalance CNW. The SVD of $\left[\boldsymbol{\mathcal{S}}_{(\Gamma_0,\Gamma)}\right]$ at $f = 100$ Hz is shows in Fig. 7 and Fig. 8. The imbalance of the CNW for quadratic and cubic elements will produce "zero" dots in the columns of the matrix $[\mathbf{V}]$ as seen in Fig. 8. Notice that the plots of the columns of $[\mathbf{U}]$ show that these modes are smooth.

6.1.2 direct regularization methods in action

It was found in the previous section that the use of higher order elements will have a negative influence in the inverse problem. For that reason we will just consider discretizations with linear elements. In this section we will include noise to the measurements and study the effect of noise in the normal velocity reconstructions. Here Γ_0 and Γ are spheres of 1026 points defined as in the previous subsection, and we use the same dipole data at $f = 100$ Hz to

	Transfer Function					Single Source				
SNR	LS	TK	TKH	TSVD	CGLS	LS	TK	TKH	TSVD	CGLS
∞	8.21	8.13	8.18	8.21	8.21	11.94	7.83	11.87	11.94	11.92
40	45.54	11.17	12.29	13.64	12.94	39.92	8.03	12.13	13.80	13.26
30	> 100	15.97	15.45	17.50	16.72	> 100	9.67	13.20	16.23	15.30
20	> 100	26.50	24.10	26.96	25.85	> 100	16.94	18.60	23.94	21.75
10	> 100	42.89	38.36	39.90	40.88	> 100	31.79	30.28	35.18	35.85

Table 6. Relative error for the normal velocity reconstruction using the transfer function and single source matrix systems with different SNR levels. The reconstruction system is solved using LS inversion and different regularization methods like Tikhonov (TK), Tikhonov with High-pass filter (TKH), Truncated SVD (TSVD) and CGLS.

generate the measurements and compare the reconstructions. In Table 6 we show the normal velocity reconstruction relative errors for 2 different systems of the NAH problem, like the transfer function in Equation 53 and the single source in Equations 57-58. For each system we use the conventional LS solution Equation 77 and 4 regularization methods: Tikhonov (TK), Tikhonov with Highpass (TKH), Truncated SVD (TSVD) and CGLS. In each regularization method we utilize the optimal regularization parameter, i.e., the regularization parameter with minimal relative error. Notice that when a lower SNR noise is added, then the errors dominate in the LS solution. For that reason is important to use regularization methods to obtain useful reconstructions.
Finally in tables 7 and 8 solve the same systems than Table 6 using the regularization parameter choice methods discussed in section 5.3: Morozov's discrepancy principle (MDP), Generalized Cross Validation (GCV) and L-curve (LC).

SNR	Tikhonov			Tikhonov with Highpass			TSVD	
	MDP	GCV	LC	MDP	GCV	LC	MDP	GCV
∞	8.5379	8.5379	8.3218	8.2066	10.5212	8.1918	8.2066	11.3525
40	19.6985	19.6985	17.9174	12.4270	13.0708	23.9702	13.7205	13.7475
30	30.5376	30.5376	30.4623	16.0863	17.6388	42.1274	18.5756	18.5133
20	40.6067	40.6067	36.7362	23.9023	25.0874	47.7316	27.0894	27.1740
10	56.3087	56.3087	42.6911	42.9117	39.5407	44.1020	44.7310	41.4242

Table 7. Relative error for the normal velocity reconstruction using the transfer function matrix system with different regularization methods and Morozov's Discrepancy Principle (MDP), Generalized Cross-Validation (GCV) and L-curve (LC) regularization parameter choice rule.

6.2 BEM and ESM

As shown in the previous subsections, the BEM produces accurate reconstructions in noise-less examples. When the measurements are contaminated by noise, then this accuracy is lost and these methods can be compared to the ESM. We utilize the same setup for Γ_0 and Γ as in the previous subsection, and we define Γ_s as a sphere of radius 0.9 m (since the maximum diameter between triangular elements is about 10 cm) with the same point distributions as Γ. As in the previous subsections we use the same dipole data at $f = 100$ Hz to generate the measurements and compare the reconstructions. In Table 9 we show the normal velocity reconstruction relative errors for 2 different methods for the NAH problem, the single source with the modified BEM approach in Equations 64-65, and the the single source with

SNR	Tikhonov			Tikhonov with Highpass			TSVD	
	MDP	GCV	LC	MDP	GCV	LC	MDP	GCV
∞	11.7515	11.7515	11.7593	11.9404	12.4217	11.8831	11.9404	12.8008
40	18.6586	18.6586	16.8357	12.8603	13.8236	22.4443	14.0582	14.0609
30	27.7760	27.7760	26.7282	13.8372	16.4718	38.9839	17.1767	17.4955
20	37.9266	37.9266	31.9003	20.4552	22.4737	45.1214	28.7443	26.0270
10	51.3872	51.3872	32.2178	42.4343	34.2850	42.9328	51.8863	40.0332

Table 8. Relative error for the normal velocity reconstruction using the single source matrix system with different regularization methods and Morozov's Discrepancy Principle (MDP), Generalized Cross-Validation (GCV) and L-curve (LC) regularization parameter choice rule.

ESM in Equations 70-71. For each system we use the conventional LS solution Equation 77 and 4 regularization methods: Tikhonov (TK), Tikhonov with Highpass (TKH), Truncated SVD (TSVD) and CGLS. In each regularization method we utilize the optimal regularization parameter. Notice that we get similar results than the previous section.

	Modified BEM Single Source					ESM Single Source				
SNR	LS	TK	TKH	TSVD	CGLS	LS	TK	TKH	TSVD	CGLS
∞	0.06	0.24	0.18	0.06	0.32	1.28	1.20	1.27	1.28	1.27
40	28.32	4.85	4.65	5.03	4.87	31.86	4.60	4.37	4.91	4.59
30	92.41	9.59	9.36	10.51	9.92	>100	8.81	8.32	9.57	8.97
20	>100	20.06	19.29	21.31	20.24	>100	18.67	17.33	18.89	17.84
10	>100	36.65	36.15	39.10	38.07	>100	33.88	32.84	35.71	34.46

Table 9. Relative error for the normal velocity reconstruction using the modified BEM single source system and ESM single source matrix systems with different SNR levels. The reconstruction system is solved using LS inversion and different regularization methods like Tikhonov (TK), Tikhonov with High-pass filter (TKH), Truncated SVD (TSVD) and CGLS.

SNR	Tikhonov			Tikhonov with Highpass			TSVD	
	MDP	GCV	LC	MDP	GCV	LC	MDP	GCV
∞	1.2698	1.2698	1.2698	1.2756	1.2739	1.2754	1.2756	1.2791
40	5.2121	5.2121	6.4921	6.4214	4.4152	8.4317	7.0922	5.0159
30	10.3119	10.3119	10.4154	16.6583	8.9566	12.4129	17.5379	9.6286
20	18.9262	18.9262	18.1611	33.9335	17.2431	18.0954	35.3276	19.7559
10	33.2015	33.2015	38.4855	51.4125	31.7035	33.0507	54.2738	35.1825

Table 10. Relative error for the normal velocity reconstruction using ESM single source matrix system with different regularization methods and Morozov's Discrepancy Principle (MDP), Generalized Cross-Validation (GCV) and L-curve (LC) regularization parameter choice rule.

In Table 10 the reconstruction error is given for the ESM single source matrix system as in Table 9 using the regularization parameter choice methods discussed in section 5.3: Morozov's discrepancy principle (MDP), Generalized Cross Validation (GCV) and L-curve (LC). Finally Fig. 9 shows the semi-convergence phenomena discussed in section 5.2, by plotting the normal velocity reconstruction relative error vs iteration of the CGLS method for the modified BEM single source system. Notice that we plot the optimal iteration and the iteration found by the Hanke-Raus method for different SNR.

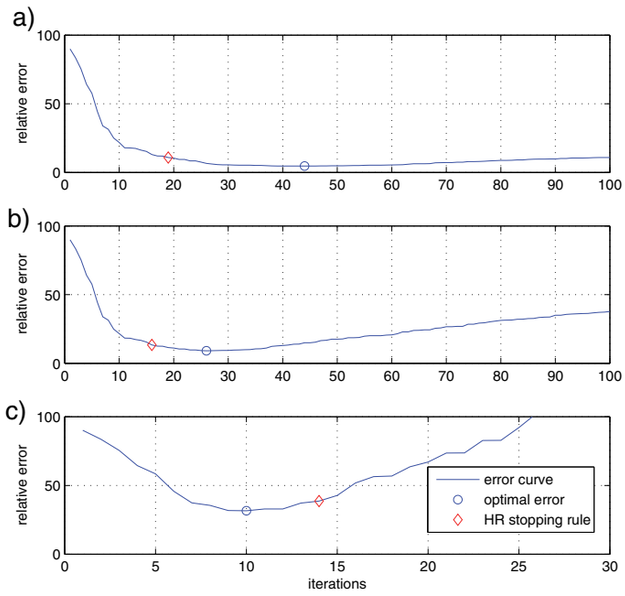


Fig. 9. Normal velocity reconstruction error vs CGLS iteration. a) 40 dB SNR, b) 30 dB SNR, and c) 10 dB SNR.

7. Acknowledgment

This work was supported by the Office of Naval Research.

8. References

Atkinson, K. E. (1997). *The Numerical Solution of Integral Equations of the Second Kind*, Cambridge University Press, New York, NY.

Augusztinovicz, F. (1999). Application and extension of acoustic holography techniques for tire noise investigations, *J. Acoust. Soc. Am.* 105 A: 1373.

Bai, M. R. (1992). Application of bem (boundary element method)-based acoustic holography to radiation analysis of sound sources with arbitrarily shaped geometries, *J. Acoust. Soc. Am.* 92: 533–549.

Borgiotti, G., Sarkissian, A., Williams, E. G. & Schuetz, L. (1990). Generalized nearfield acoustic holography for axisymmetric geometries, *J. Acoust. Soc. Am.* 88: 199–209.

Calvetti, D., Lewis, B. & Reichel, L. (2001a). GMRES, L-curves, and discrete ill-posed problems, *BIT* 42(1): 44–65.

Calvetti, D., Lewis, B. & Reichel, L. (2001b). On the choice of subspace for iterative methods for linear discrete ill-posed problems, *Int.J.Appl.Math.Comput.Sci.* 11(5): 1069–1092.

Calvetti, D., Lewis, B. & Reichel, L. (2002). On the regularizing properties of GMRES, *Numer. Math.* 91(4): 605–625.

Chien, D. (1995). Numerical evaluation of surface integrals in three dimensions, *Mathematics of Computation* 64(210): 727–743.

Colton, D. & Kress, R. (1983). *Integral Equation Methods in Scattering Theory*, Wiley-Interscience Publication, New York, NY.

Colton, D. & Kress, R. (1992). *Inverse Acoustics and Electromagnetic Scattering Theory*, Springer-Verlag, New York, NY, p. pp. 19.

Delillo, T. K., Isakov, V., Valdivia, N. & Wang, L. (2000). Computational methods for the detection of the source of acoustical noise, *Proceedings of ASME2000*, Orlando, Florida.

DeLillo, T. K., Isakov, V., Valdivia, N. & Wang, L. (2001). The detection of the source of acoustical noise in two dimensions, *SIAM Journal of Applied Math.* 61(6): 2104–2121.

DeLillo, T. K., Isakov, V., Valdivia, N. & Wang, L. (2003). The detection of surface vibrations from interior acoustical pressure, *Inverse Problems.* 19(3): 507–524.

Engl, H. W., Hanke, M. & Neubauer, A. (1996). *Regularization of Inverse Problems*, Kluwer Academic Publishers, Boston.

Hanke, M. (1995). *Conjugate Gradient Methods for Ill-Posed Problems*, Kluwer Academic Publishers, Boston.

Hanke, M. & Raus, T. (1996). A general heuristic for choosing the regularization parameter in ill-posed problems, *SIAM J. Sci. Comput.* 17(4): 956–972.

Hansen, P. C. (1998). *Rank-Deficient and Discrete Ill-Posed Problems*, Siam, Philadelphia, PA, chapter 5-6.

Hansen, P. & O'Leary, D. (1993). The use of the l-curve in the regularization of discrete ill-posed problems, *SIAM J. Sci. Comput.* 14(6): 341–373.

Kang, S.-C. & Ih, J.-G. (2000a). On the accuracy of nearfield pressure predicted by the acoustic boundary element method, *J. Sound Vib.* 233: 353–358.

Kang, S.-C. & Ih, J.-G. (2000b). The use of partially measured source data in near-field acoustical holography based on the bem, *J. Acoust. Soc. Am.* 107: 2472–2479.

Kang, S.-C. & Ih, J.-G. (2001). Use of nonsingular boundary integral formulation for reducing errors due to near-field measurements in the boundary element method based near-field acoustic holography, *J. Acoust. Soc. Am.* 109: 1320–1328.

Kim, B.-K. & Ih, J.-G. (1996). On the reconstruction of the vibro-acoustic field over the surface enclosing an interior space using the boundary element method, *J. Acoust. Soc. Am.* 100: 3003–3016.

Kim, B.-K. & Ih, J.-G. (2000). Design of an optimal wave-vector filter for enhancing the resolution of reconstructed source field by nah, *J. Acoust. Soc. Am.* 107: 3289–3297.

Kim, G.-T. & Lee, B.-H. (1990). 3-d sound source reconstruction and field reprediction using the helmholtz integral equation, *J. Sound Vib.* 136: 245–261.

Langrenne, C. & Garcia, A. (1999). Integral formulations for the vibroacoustic characterization of a cello, *J. Acoust. Soc. Am.* 105 A: 1088.

Maynard, J. D. (1988). Acoustic holography for wideband, odd-shaped noise sources, *Proceedings Inter-noise '88*, Avignon, France, pp. 223–231 (Volume I).

Maynard, J. D., Williams, E. G. & Lee, Y. (1985). Nearfield acoustic holography (nah), i. theory of generalized holography and the development of nah, *J. Acoust. Soc. Am.* 78: 1395–1413.

McLean, W. (2000). *Strongly Elliptic Systems and Boundary Integral Equations*, Cambridge University Press, New York.

Nelson, P. A. & Yoon, S. H. (2000). Estimation of acoustic source strength by inverse methods: Part i, conditioning of the inverse problem, *J. Sound Vib.* 233: 643–668.

Ouellet, D., Guyader, J. L. & Nicolas, J. (1991). Sound field in a rectangular cavity in the presence of a thin, flexible obstacle by integral equation method, *J. Acoust. Soc. Am.* 89: 2131–2139.

Pan, J. & Bies, D. A. (1990). The effect of fluid-structural coupling on sound waves in a enclosure - theoretical part, *J. Acoust. Soc. Am.* 87: 691–707.

Raveendra, S. T., Vlahopoulos, N. & Glaves, A. (1998). An indirect boundary element formulation for multi-valued impedance simulation in structural acoustics, *App. Math. Modelling* 22: 379–393.

Sarkissian, A. (1990). Near-field acoustical holography for an axisymmetric geometry: a new formulation, *J. Acoust. Soc. Am.* 88: 961–966.

Sarkissian, A., Gaumond, C. F., Williams, E. G. & Houston, B. H. (1993). Reconstruction of the acoustic field over a limited surface area on a vibrating cylinder, *J. Acoust. Soc. Am.* 93: 48–54.

Schuhmacher, A., Hald, J., Rasmussen, K. B. & Hansen, P. C. (2003). Sound source reconstruction using inverse boundary element calculations, *J. Acoust. Soc. Am.* 113(1): 114–126.

Schwab, C. & Wendland, W. L. (1992). On numerical cubatures of singular surface integrals in boundary element methods, *Numerische Mathematik* 62(3): 343–369.

Seybert, A. F., Soenarko, B., Rizzo, F. J. & Shippy, D. J. (1985). An advanced computational method for radiation and scattering of acoustic waves in three dimensions, *J. Acoust. Soc. Am.* 77: 362–368.

Strout, A. (1971). *Approximate Calculation of Multiple Integrals*, Prentice-Hall, New Jersey.

Sureshkumar, S. & Raveendra, S. T. (2001). An analysis of regularization errors in generalized nearfield acoustical holography, *2001 SAE noise and vibration conference*, number 2001-01-1616, Grand Traverse, MI.

Tekatlian, A., Filippi, P. & Habault, D. (1996). Determination of vibration characteristics of noise sources solving an inverse radiation problem, *Acustica* 82: 91–101.

Valdivia, N. & Williams, E. G. (2005). Krylov subspace iterative methods for boundary element method based near-field acoustic holography, *J. Acoust. Soc. Am.* 117(2).

Valdivia, N. & Williams, E. G. (2006). Study of the comparison of the methods of equivalent sources and boundary element methods for near-field acoustic holography, *J. Acoust. Soc. Am.* 120(6).

Veronesi, W. A. & Maynard, J. D. (1989). Digital holographic reconstruction of sources with arbitrarily shaped surfaces, *J. Acoust. Soc. Am.* 85: 588–598.

Vlahopoulos, N. & Raveerdra, S. T. (1998). Formulation, implementation and validation of multiple connection and free edge constraints in a indriect boundary element formulation, *J. Sound Vib.* 201: 137–152.

Williams, E. G. (1997). On green functions for a cylindrical cavity, *J. Acoust. Soc. Am.* 102: 3300–3307.

Williams, E. G. (1999). *Fourier Acoustics: Sound Radiation and Nearfield Acoustical Holography*, Academic Press, London, UK, chapter 3.

Williams, E. G. (2001). Regularization methods for near-field acoustical holography, *J. Acoust. Soc. Am.* 110: 1976–1988.

Williams, E. G., Houston, B. H., Herdic, P. C., Raveendra, S. T. & Gardner, B. (2000). Interior NAH in flight, *J. Acoust. Soc. Am.* 108: 1451–1463.

Williams, E. G. & Maynard, J. D. (1980). Holographic imaging without the wavelength resolution limit, *Phys. Rev. Lett.* 45: 554–557.

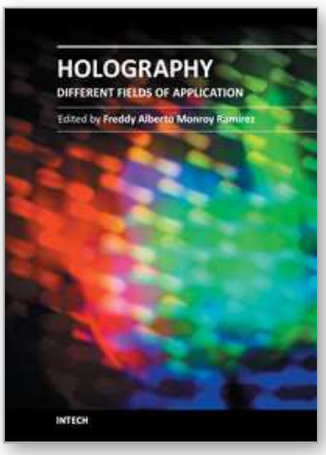
Wu, S. F. & Zhao, X. (2002). Combined helmholtz equation-least squares method for reconstructing acoustic radiation from arbitrarilty shaped objects, *J. Acoust. Soc. Am.* 112: 179–188.

Yoon, S. H. & Nelson, P. A. (2000). Estimation of acoustic source strength by inverse methods: Part ii, experimental investigation of methods for choosing regularization parameters, *J. Sound Vib.* 233: 669–705.

Zhang, Z., Vlahopoulos, N., Allen, T. & Zhang, K. Y. (2001). A source reconstruction process based on a indirect variational boundary element formulation, *Engineering Analysis with Boundary Elements* 25: 93–114.

Zhang, Z., Vlahopoulos, N., Raveendra, S. T., Allen, T. & Zhang, K. Y. (2000). A computational acoustic field reconstruction process based on a indirect boundary element formulation, *J. Acoust. Soc. Am.* 108: 2167–2178.

IntechOpen



Holography - Different Fields of Application

Edited by Dr. Freddy Monroy

ISBN 978-953-307-635-5
Hard cover, 148 pages
Publisher InTech
Published online 12, September, 2011
Published in print edition September, 2011

This book depicts some differences from the typical scientific and technological literature on the theoretical study of holography and its applications. It offers topics that are not very commercial nor known, which will allow a different view of the field of optics. This is evident in chapters such as â€œElectron Holography of Magnetic Materialsâ€, â€œPolarization Holographic Gratings in Polymer Dispersed Formed Liquid Crystals, and â€œDigital Holography: Computer-generated Holograms and Diffractive Optics in Scalar Diffraction Domainâ€. The readers will gain a different view of the application areas of holography and the wide range of possible directions that can guide research in the fields of optics.

How to reference

In order to correctly reference this scholarly work, feel free to copy and paste the following:

Nicolas P. Valdivia (2011). Numerical Methods for Near-Field Acoustic Holography over Arbitrarily Shaped Surfaces, Holography - Different Fields of Application, Dr. Freddy Monroy (Ed.), ISBN: 978-953-307-635-5, InTech, Available from: http://www.intechopen.com/books/holography-different-fields-of-application/numerical-methods-for-near-field-acoustic-holography-over-arbitrarily-shaped-surfaces

INTECH
open science | open minds

InTech Europe
University Campus STeP Ri
Slavka Krautzeka 83/A
51000 Rijeka, Croatia
Phone: +385 (51) 770 447
Fax: +385 (51) 686 166
www.intechopen.com

InTech China
Unit 405, Office Block, Hotel Equatorial Shanghai
No.65, Yan An Road (West), Shanghai, 200040, China
中国上海市延安西路65号上海国际贵都大饭店办公楼405单元
Phone: +86-21-62489820
Fax: +86-21-62489821

© 2011 The Author(s). Licensee IntechOpen. This chapter is distributed under the terms of the Creative Commons Attribution-NonCommercial-ShareAlike-3.0 License, which permits use, distribution and reproduction for non-commercial purposes, provided the original is properly cited and derivative works building on this content are distributed under the same license.

IntechOpen

IntechOpen